Genetic variation in the species *Arabidopsis thaliana* reveals the existence of natural heat resilience factors for meiosis

Jiayi Zhao[1], Huiqi Fu[1], Zhengze Wang[2], Min Zhang[1], Yaoqiong Liang[1], Xueying Cui[1], Wenjing Pan[1], Ziming Ren[3], Zhihua Wu[4], Yujie Zhang[1], Xin Gui[1], Li Huo[1], Xiaoning Lei[5], Chong Wang[6], Arp Schnittger[7], Wojciech P. Pawlowski[8], Bing Liu[1,*]

1 Arameiosis Lab, South-Central Minzu University, Wuhan 430074, China;

2 College of Life Science and Technology, Huazhong Agricultural University, Wuhan 430070, China;

3 Department of Landscape Architecture, Zhejiang Sci-Tech University, Hangzhou 310018, China;

4 College of Life Sciences, Zhejiang Normal University, Jinhua 321004, China;

5 School of Public Health, Shanghai Jiao Tong University School of Medicine, Shanghai 200025, China;

6 Shanghai Key Laboratory of Plant Molecular Sciences, Development Center of Plant Germplasm Resources, College of Life Sciences, Shanghai Normal University, Shanghai 200234, China;

7 Department of Developmental Biology, University of Hamburg, Hamburg 22609, Germany;

8 School of Integrative Plant Science, Cornell University, Ithaca, NY 14853, USA.

* To whom correspondence should be addressed: Bing Liu (arameiosis@163.com)

Abstract

Heat interferes with multiple meiotic processes leading to genome instability and sterility in flowering plants, including many crops. Despite its importance for food security, the mechanisms underlying heat tolerance of meiosis are poorly understood. In this study, we analyzed different meiotic processes in the Arabidopsis (*Arabidopsis thaliana*) accessions Columbia (Col) and Landsberg *erecta* (L*er*), their F1 hybrids and F2 offspring under heat stress (37°C). At 37°C, Col exhibits significantly reduced formation of double-stand breaks (DSBs) and completely abolished homolog pairing, synapsis and crossover (CO) formation. Strikingly, L*er* and L*er*/Col hybrids are much less affected than Col. Interestingly, only 10% ~ 20% of F2 offspring exhibit the same heat tolerance of meiotic recombination as parents, indicating that heat resilience in L*er* is controlled by the interplay of several loci. Moreover, F2 offspring show defective chromosome condensation in interkinesis, and untimely sister-chromatid segregation and/or chromosome fragmentation, the levels of which exceed those in either inbreds and/or hybrids thus implying a transgressive effect on heat tolerance of meiosis. Furthermore, correlation and cytogenetic analysis suggest that homolog pairing and/or synapsis have an impact on heat tolerance of chromosome morphology and stability during post-recombination stages under heat stress. Taken together, this study reveals the existence of natural heat resilience factors for meiosis in Arabidopsis, which have the great potential to be exploited in breeding programs.

Author summary

Environmental temperature alterations affect meiotic recombination and/or chromosome segregation thus perturbing genetic makeup and genome stability in plants. We have previously reported that CO formation is fully abolished in *Arabidopsis thaliana* accession Col under heat stress (36°C-38°C) due to reduced DSB formation and impaired homolog pairing. Here, we show that in *Arabidopsis thaliana* accession L*er* under the same high temperature conditions, both DSB and CO formation occur normally, and homolog pairing is mildly impacted, which indicate a striking difference in

heat tolerance of meiotic recombination from Col. Remarkably, Col/L*er* hybrids display the same heat tolerance as L*er*, however, only 10% ~ 20% of F2 offspring behave the same as parents. Moreover, we found higher levels of defects in chromosome morphology and integrity, and sister-chromatid segregation in F2 population than those in both inbreds and hybrids, which suggest a transgressive effect influencing heat tolerance of meiosis. Our findings reveal that heat resilience in Arabidopsis is controlled by the interplay of multiple genomic loci, holding a great potential to be exploited in crop breeding.

Introduction

Meiosis is a specialized type of cell division, which, in plants, generates spores with halved chromosome number required for sexual reproduction and maintenance of ploidy consistency over generations. During prophase I, homologous chromosomes (homologs) undergo recombination, resulting in reciprocal exchange of DNA fragments and thereby promoting genetic diversity. Meiotic recombination is initiated by the programmed formation of DNA double-strand breaks (DSBs) catalyzed by the conserved topoisomerase VI-like protein SPO11 together with other components of the DSB formation machinery (1, 2). The recombinases RAD51 and DMC1 catalyze DSB repair via homologous recombination (3-5). In plants, deficiencies in DSB repair result in impaired crossover (CO) formation and/or cause chromosome fragmentation (3-6). Although a large number of DSBs is generated along chromosomes, only a small proportion of them are repaired into COs. In Arabidopsis as in many other species, most COs are catalyzed by the ZMM proteins resulting in type-I COs that are placed at a distance from each other (CO interference) (7). The formation of the remaining approximately 15% of COs in plants involves structure-selective endonucleases such as MUS81 giving rise to type-II COs, which are typically not subject to CO interference (8). The process of COs formation can be visualized by the linking of homologs giving rise to bivalents connected by chiasmata. In the wild-type, all homologs become eventually connected through at least one CO (CO assurance) (9), which is required for equal

63 distribution of homologs after meiosis I. During meiotic recombination, chromatids are organized into loops, which
64 are anchored to the chromosome axis through the interactions between axis core proteins (e.g. ASY3 and ASY4 in
65 Arabidopsis) and the axis-associated HORMA domain protein ASY1 (10-13). The assembly of the chromosome axis is
66 required for normal DSB formation and repair, homolog pairing and synapsis, and recombination (12, 14-16).
67
68 The separation of homologs and sister chromatids is facilitated by spindles. Cohesin, a ring-shaped protein complex,
69 assures the protection of the sister-chromatids union. The cohesion on chromosome arms is released during prophase
70 and particularly during anaphase I allowing the separation of homologs (17). The centromeric cohesion is removed in
71 anaphase II paving the road for the segregation of sister chromatids (18). The function and stability of centromeres
72 are crucial for maintenance of cohesion and thus faithful chromosome segregation (19, 20).
73
74 Several studies have shown that meiosis in plants is sensitive to temperature variations (21-25). Either elevated or
75 reduced temperature can interfere with cytoskeleton organization and/or meiotic cell cycle transition resulting in
76 defective cytokinesis and unreduced spores (26-30). In Arabidopsis, mildly decreased or increased temperature within
77 the spectrum that does not reduce fertility (8-28°C) promotes type-I CO formation (31, 32). Higher temperatures (30-
78 34°C), however, attenuate homolog synapsis and alter CO rate and distribution, affecting meiosis progression (25, 30).
79 In addition, increased temperatures perturb stability of centromeres and induce unbalanced chromosome segregation
80 in Arabidopsis (33-35). At extremely high temperatures (36-38°C), homolog pairing and synapsis and CO formation in
81 the Arabidopsis accession Columbia (Col) is completely abolished, which results in disrupted chromosome segregation
82 and sterility (36-38). Despite the significance of heat stress on genetic makeup and genome stability in plants, the
83 molecular mechanisms controlling heat tolerance of meiosis remain poorly understood.
84

85 Interestingly, previous studies have shown that there are naturally existing genetic differences with respect to meiotic
86 recombination and stress tolerance in plants (39-45). Here, we report that the *Arabidopsis thaliana* accessions Col and
87 Landsberg *erecta* (L*er*) show striking differences in heat tolerance of meiotic recombination. Our data reveal that
88 meiotic chromosome stability in Col/L*er* F2 progeny is more sensitive to heat than in either inbreds or their hybrids
89 indicating that several loci contribute to the natural heat resistance.
90

91 **Results**

92 **Landsberg *erecta* exhibits higher heat tolerance of meiosis than Columbia**

93 The *Arabidopsis thaliana* accessions Columbia (Col) and Landsberg *erecta* (L*er*), two frequently used varieties, exhibit
94 differences in their meiotic recombination rates as well as response to stresses (39, 42, 45-48). To test whether heat
95 tolerance of meiosis also varies, we compared the effect of extreme heat stress, i.e., 37°C, versus the control condition,
96 i.e., 20°C, on these two accessions. To this end, we analyzed tetrad formation at the end of meiosis by orcein staining.
97 At 20°C, both accessions generated typical tetrads that harbored four spores with equally-sized nuclei (Fig 1a and b).
98 Exposure to the extreme temperature resulted in 85.7% tetrads in Col that showed irregular configurations with
99 abnormal numbers and/or sizes of spores and nuclei (Fig 1a and b). In striking contrast, only 8.8% abnormal tetrads
100 were found in L*er* (Fig 1a and b), suggesting that meiosis in L*er* is more resilient to heat stress than Col.
101

102 Heat-induced formation of abnormal tetrads could result from defective meiotic recombination that leads to
103 univalents and consequently, chromosome mis-segregation. Alternatively, defects in microtubule-mediated
104 chromosome distribution and/or cytokinesis could be the underlying cause (38). To determine which meiotic process
105 in Col is more affected by heat stress, we analyzed the spindle at metaphase I and II as well as phragmoplast at
106 telophase II (27, 38, 49). At 20°C, the typical barrel-shaped spindles and straight phragmoplasts were observed in both

107 accessions (Fig 1c). At 37°C, we did not observe obvious defects in microtubule organization in prophase I meiocytes
108 in either accession (Fig S1) while Col and L*er* showed similar rates of irregularities in morphology of spindles and
109 phragmoplasts in meiosis I and/or II (Fig 1d, normal; e, abnormal; and f) that likely contributed to an unequal
110 segregation of chromosomes (Fig 1g). The higher heat tolerance of meiosis in L*er* versus Col is thus likely not caused
111 by the difference in microtubule organization, but possibly occurs prior to metaphase I, i.e., meiotic recombination.
112

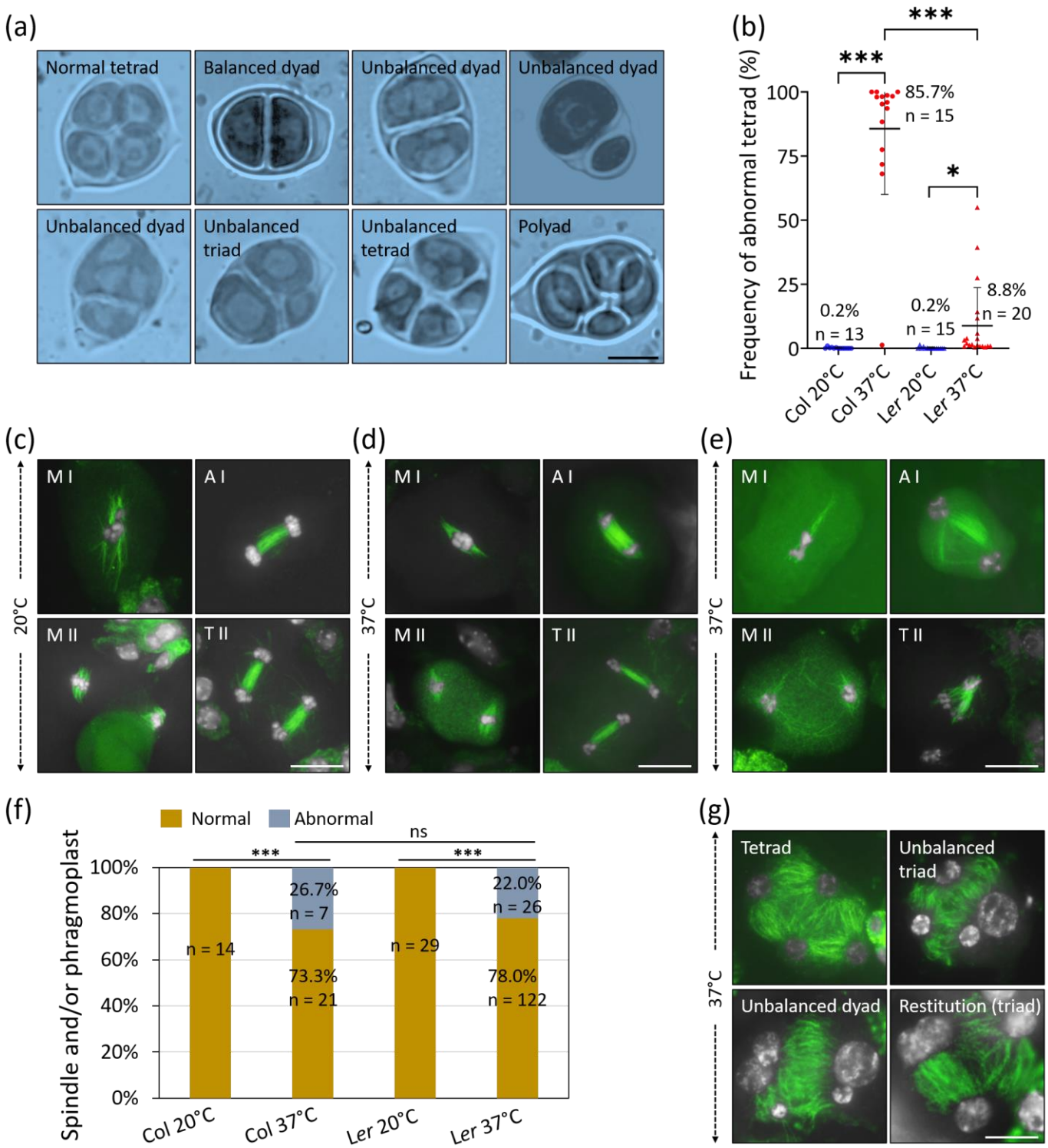

Figure 1. L*er* exhibits a higher heat tolerance of meiosis than Col. (a) Representative images of tetrads with normal or abnormal configurations. (b) Graph showing the frequencies of abnormal tetrads in Col and L*er* at 20°C or 37°C. Stars indicate significance levels based on unpaired *t* tests. (c and d) Representative images of immunolocalization of α-tubulin in metaphase I, anaphase I, metaphase II and telophase II meiocytes depicting normal microtubule configurations at 20°C (c) or 37°C (d). (e) Representative

118 images of immunolocalization of α-tubulin in metaphase I, anaphase I, metaphase II and telophase II meiocytes displaying altered
119 configurations at 37°C. (f) Graph showing the rates of spindle and phragmoplast with normal or abnormal configurations in Col
120 and L*er* at 20°C or 37°C. Stars indicate significance levels based on χ^2-tests. (g) Representative images of immunolocalization of α-
121 tubulin in tetrads showing normal or abnormal configurations at 37°C. White, DAPI; green, α-tubulin. Frequencies represent the
122 average rates of the corresponding phenotypes; n indicates the number of the analyzed plants or meiocytes; ***, $P < 0.001$; *, P
123 < 0.05; ns, $P > 0.05$; scale bars, 10 μm.
124

125 **DSB and CO formation in L*er* are largely resistant to heat**

126 To assess the possible resilience of meiotic recombination towards heat in L*er*, we analyzed chromosomes by spreading
127 and scored bivalent formation in Col and L*er* at 20°C and 37°C. At 20°C, five bivalents were present in diakinesis in both
128 accessions (Fig 2a and c). While bivalent formation in Col was completely impaired at 37°C, this was not the case in L*er*
129 (Fig 2a and c). To examine then the effect of heat on CO formation, immunolocalization of the type-I CO marker protein
130 HEI10 was performed and the number of HEI10 foci on chromosomes in diakinesis was quantified. At 20°C, as
131 previously reported, Col showed a higher number of HEI10 foci than L*er* with 11.0 foci versus 9.4, respectively (Fig 2b
132 and d) (45). At 37°C, no HEI10 foci were detected in Col whereas L*er* showed an average of 10.5 HEI10 foci per meiocyte,
133 being not significantly different from the number at 20°C (Fig 2b and d). Moreover, all analyzed anaphase I meiocytes
134 in heat-stressed Col showed mis-segregation of homologs while only 41.5% unequal homolog segregation occurred in
135 L*er* under heat stress (Fig 2e and f). Based on these data, we conclude that heat stress does not reduce CO formation
136 in L*er*. Since heat stress has earlier been found to partially suppress CO formation by reducing DNA double-strand
137 break (DSB) formation (36), we next analyzed the localization of the DSB repair recombinases RAD51 and DMC1, two
138 widely used DSB markers (5, 50). Consistent with previous reports, both the numbers of RAD51 and DMC1 foci on
139 zygotene chromosomes in Col were significantly reduced after heat treatment (Fig 2g-j) (36, 51). In L*er*, however, the

140 focus numbers of both proteins were not significantly altered by heat (Fig 2g-j), suggesting that heat stress does not

141 reduce DSB formation in L*er*.

142

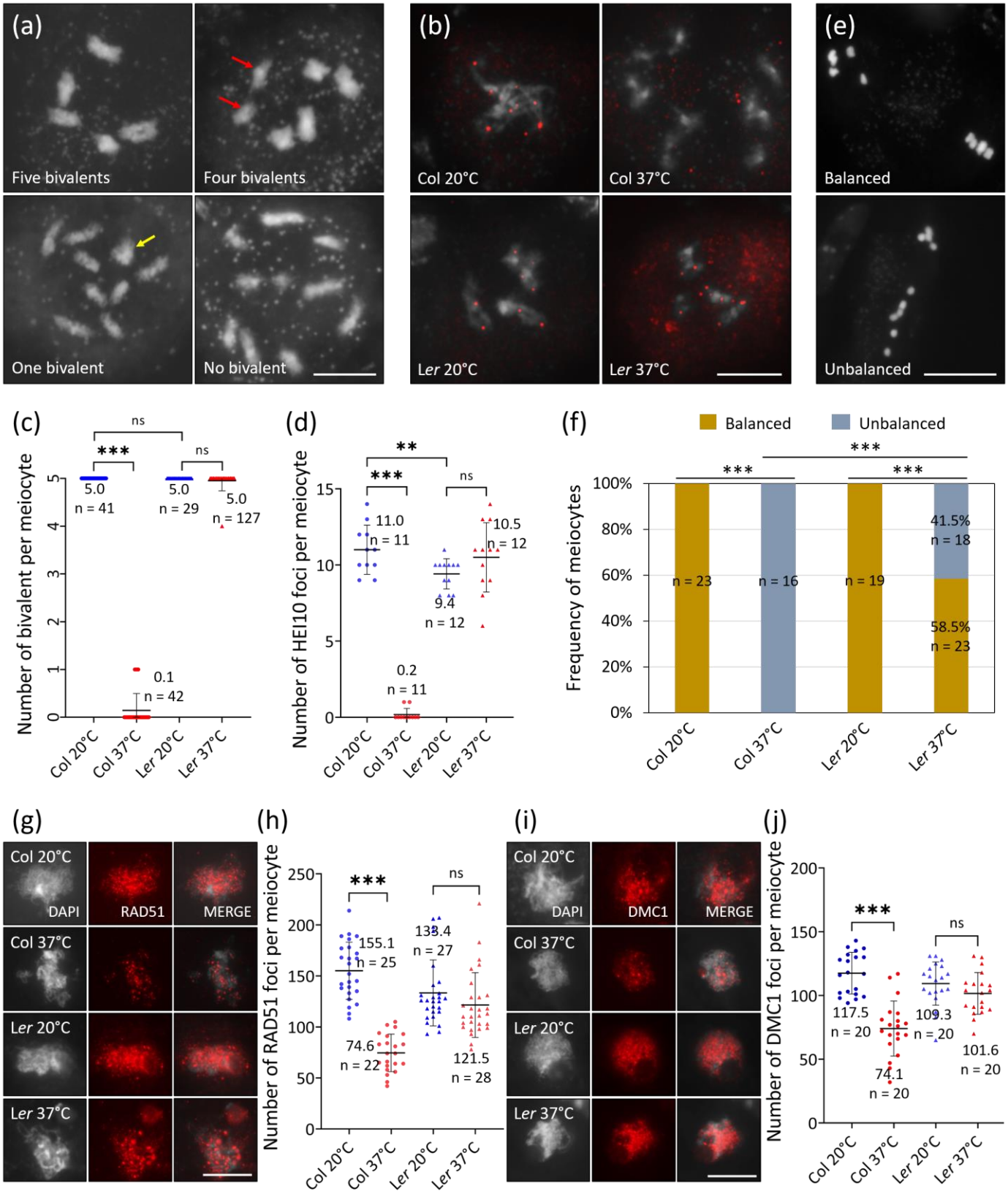

Figure 2. Heat stress does not reduce CO and DSB formation in L*er*. (a) Representative images of diakinesis meiocytes showing five, four, one or no bivalents. The red and yellow arrows indicate univalents and bivalent, respectively. (b) Immunolocalization of HEI10

146 in diakinesis meiocytes of Col and L*er* at 20°C and 37°C. (c and d) Graphs showing the average numbers of bivalent (c) and HEI10
147 foci (d) per meiocyte in Col and L*er* at 20°C and 37°C. Stars indicate significance levels based on unpaired *t* tests. (e) Representative
148 images of anaphase I meiocytes showing balanced and unequal homolog separation. (f) Graph showing the fraction of anaphase
149 I meiocytes with equal or unequal homolog separation in Col and L*er* at 20°C and 37°C. Stars provide significance levels based on
150 χ^2-tests. (g and i) Immunolocalization of RAD51 (g) and DMC1 (i) on zygotene chromosomes of Col and L*er* at 20°C and 37°C. (h
151 and j) Graphs showing the average numbers of RAD51 (h) and DMC1 (j) foci per meiocyte in Col and L*er* at 20°C and 37°C. Stars
152 indicate significance levels based on unpaired *t* tests; frequencies indicate the average number or fraction of the corresponding
153 phenotypes; n indicates the number of the analyzed cells; ***, $P < 0.001$; **, $P < 0.01$; ns, $P > 0.05$; scale bars, 10 µm.
154

155 **Homolog synapsis in L*er* is more tolerant to heat stress than in Col**

156 Disrupted homolog pairing is the main cause of impaired CO formation in Col under heat stress (36). Therefore, we
157 compared heat tolerance of homolog pairing in Col and L*er*. We classified pachytene meiocytes into three types based
158 on juxtaposition status of homologs: full-pairing, which indicates meiocytes exhibiting fully juxtaposed homologs (Fig
159 3a, b and e); partial-pairing, which indicates meiocytes showing both juxtaposed and unpaired regions between
160 homologs (Fig 3f-i); and no pairing that represents impairment of homolog juxtaposition (Fig 3c and d). As previously
161 reported, homolog pairing and synapsis in Col were fully impaired at 37°C (Fig 3a, c and j) (36). In L*er*, however, 63.1%
162 of meiocytes exhibited full pairing (Fig 3e and j), and 35.2% of meiocytes showed partial pairing (Fig 3f-i, red arrows;
163 j), with only 1.5% meiocytes displaying no pairing (Fig 3d and j). Next, we compared the impact of heat on chromosome
164 morphology and the assembly of the chromosome axis and synaptonemal complex (SC) by analyzing the localization
165 of ASY4 and ZYP1 on zygotene and pachytene chromosomes, respectively. At 20°C, ASY4 were loaded on the whole
166 DAPI-stained chromosome regions showing a linear configuration (Fig 3k and l). Heat induced patchy ASY4 signals in
167 both Col and L*er* (Fig 3k), but the fraction of this phenotype in Col was significantly higher than that in L*er* (Fig 3l, $P <$

0.001). Immunolocalization of ZYP1 showed that the SC assembly in Col was disrupted by heat, which, however, occurred normally or was only partially perturbed in most pachytene meiocytes in L*er* (Fig 3m-s, and t, ~95.6%). These data indicate that homolog pairing and synapsis in L*er* are less impacted by heat than in Col.

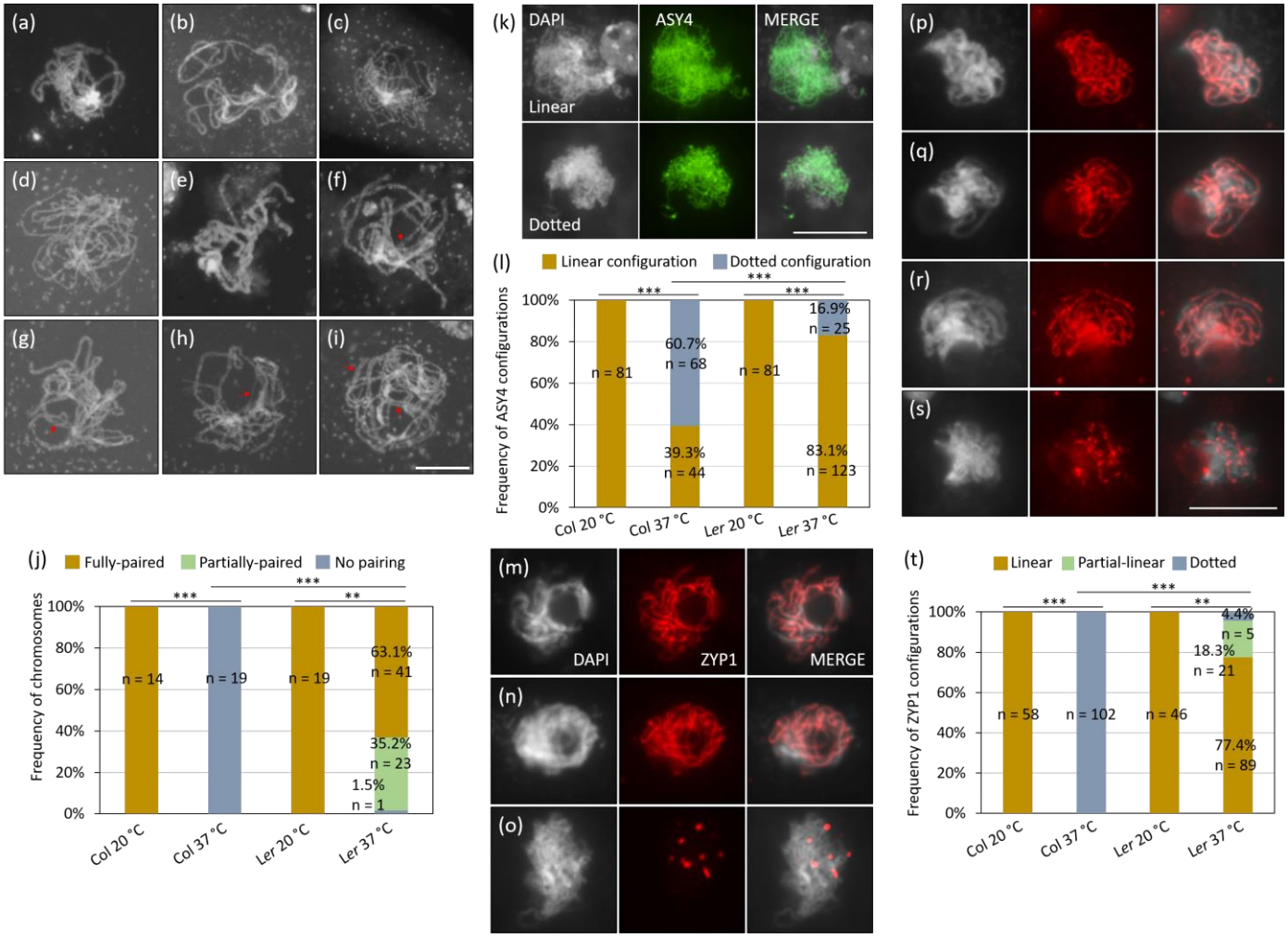

Figure 3. Homolog pairing and synapsis in L*er* are less impacted by heat than those in Col. (a-i) Pachytene chromosomes in Col (a and c) and L*er* (b, d-i) at 20°C (a and b) and 37°C (c-i). The red arrows indicate unpaired chromosome regions. (j) Graph showing the rates of pairing status of pachytene chromosomes in Col and L*er* at 20°C and 37°C. Stars indicate significance levels based on χ^2-tests. (k) Representative images of immunolocalization of ASY4 on chromosomes showing linear or patchy configurations. White, DAPI; green, ASY4. (l) Graph showing the rates of ASY4 configurations in Col and L*er* at 20°C and 37°C. Stars indicate significance levels based on χ^2-tests. (m-s) Immunolocalization of ZYP1 on pachytene chromosomes in Col (m and o) or L*er* (n, p-s) at 20°C (m

179 and n) and 37°C (o-s). White, DAPI; red, ZYP1. (t) Graph showing the rates of ZYP1 configurations on pachytene chromosomes in
180 Col and L*er* at 20°C and 37°C. Stars indicate significance levels based on χ^2-tests; frequencies indicate the rates of the corresponding
181 phenotypes; n indicates the number of the analyzed cells; ***, $P < 0.001$; **, $P < 0.01$; scale bars, 10 µm.
182
183 **Col/L*er* hybrids exhibit similar heat tolerance of meiotic recombination as L*er***
184 One of the main developmental differences between Col and L*er* is floral architecture (Fig S2), which, in Arabidopsis,
185 is regulated by the receptor-like protein kinase ERECTA (ER) that acts upstream of the mitogen-activated protein kinase
186 cascade module MKK4/5-MPK3/6 (52, 53). In addition, ER potentially plays a role in varied heat responses between
187 Col and L*er* (54, 55). We thus examined whether the distinct heat tolerance of meiotic recombination between Col and
188 L*er* is owing to a loss of *ER*. To this end, we analyzed bivalent formation, homolog separation, DMC1 and ASY4
189 localization, pachytene chromosome morphology as well as the SC assembly in Col plants defective for ER and/or MPK6.
190 Both the single *er* and *mpk6* and the double *er mpk6* mutants displayed the same heat tolerance of meiotic
191 recombination as Col (Fig 4d, f, h, j and n).
192
193 To further explore the impact of the general genetic background on heat tolerance of meiosis, we analyzed
194 chromosome behavior in heat-stressed Col/L*er* hybrids, which exhibited the same flower architecture as Col (Fig S2).
195 These plants produced a lower level of abnormal tetrads (~31.0%) than Col (Fig 4a and b; Fig 1b; $P < 0.001$). Interestingly,
196 bivalent formation in Col/L*er* hybrids was not reduced under heat stress (Fig 4c and d), supporting the conclusion that
197 heat tolerance of meiotic recombination in L*er* is not conferred by the flower architecture. In addition, balanced
198 homolog segregation at anaphase I in heat-stressed Col/L*er* hybrids occurred at a similar frequency as in L*er* (Fig 4e
199 and f; Fig 2f; $P > 0.05$). Moreover, at 37°C, zygotene chromosomes in Col/L*er* hybrids showed an average number of
200 DMC1 foci (~116.0) significantly higher than those observed for Col (~74.1; $P < 0.001$) and L*er* (~101.6; $P < 0.05$) (Fig

201 4g and h; Fig 2j). Analysis of pachytene chromosome configurations and ASY4 localization revealed no significant
202 difference in heat tolerance between Col/L*er* hybrids and L*er* (Fig 4i-l; Fig 3j and l; $P > 0.05$). Furthermore, most
203 pachytene meiocytes (~74.1%) in Col/L*er* hybrids displayed a partial linear localization pattern of ZYP1, the extent of
204 which was higher than that in L*er* (Fig 4m and n; Fig 3t; $P < 0.001$); and the meiocytes showing linear or patchy ZYP1
205 localization occupied 1.8% and 24.1%, respectively (Fig 4m and n). Overall, these findings revealed similar heat
206 tolerance of meiotic recombination in Col/L*er* hybrids and in L*er*.
207

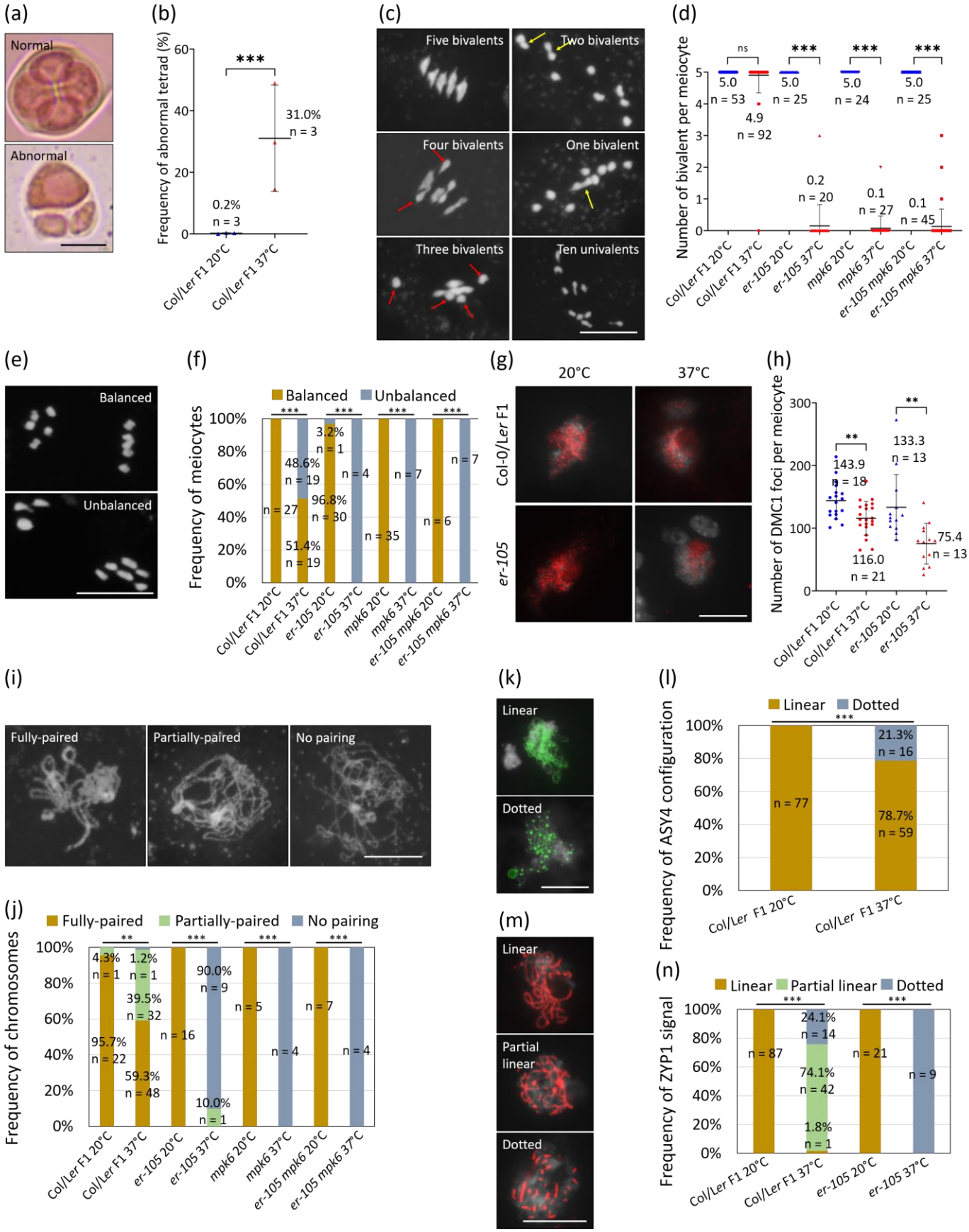

208

209 Figure 4. Col/*Ler* hybrids exhibit similar heat tolerance of meiotic recombination as *Ler*. (a) Representative images of normal and

210 abnormal tetrads. (b) Graph showing the rates of abnormal tetrad in Col/L*er* hybrids at 20°C and 37°C. (c) Representative images
211 of metaphase I chromosomes with different numbers of bivalents. The red and yellow arrows indicate univalents and bivalents,
212 respectively. (d) Graph showing the average numbers of bivalent per diakinesis and/or metaphase I meiocyte in Col/L*er* hybrids,
213 the single *er-105* and *mpk6*, and the double *er-105 mpk6* mutants at 20°C and 37°C. (e) Representative images of anaphase I
214 chromosomes showing balanced or unbalanced homolog separation. (f) Graph showing the frequencies of anaphase I meiocytes
215 with balanced or unbalanced homolog separation in Col/L*er* hybrids, the single *er-105* and *mpk6*, and the double *er-105 mpk6*
216 mutants at 20°C and 37°C. (g) Immunolocalization of DMC1 on zygotene chromosomes in Col/L*er* hybrids and *er-105* at 20°C and
217 37°C. White, DAPI; red, DMC1. (h) Graph showing the average numbers of DMC1 foci per meiocyte in Col/L*er* hybrids and *er-105*
218 at 20°C and 37°C. (i) Representative images of pachytene chromosomes showing full-pairing, partial-pairing, and no pairing. (j)
219 Graph showing the rates of pachytene meiocytes exhibiting full-pairing, partial-pairing and no pairing in Col/L*er* hybrids, the single
220 *er-105* and *mpk6* and the double *er-105 mpk6* mutants at 20°C and 37°C. (k) Representative images of immunolocalization of ASY4
221 on zygotene chromosomes showing different configurations. White, DAPI; green, ASY4. (l) Graph showing the frequencies of ASY4
222 configurations in Col/L*er* hybrids at 20°C and 37°C. (m) Representative images of immunolocalization of ZYP1 on pachytene
223 chromosomes showing different configurations. White, DAPI; red, ZYP1. (n) Graph showing the rates of ZYP1 configurations on
224 pachytene chromosomes in Col/L*er* hybrids and the single *er-105* mutant at 20°C and 37°C. In (b), (d) and (h), stars indicate
225 significance levels based on unpaired *t* tests; in (f), (j), (l) and (n), stars indicate significance levels based on χ^2-tests; ***, $P < 0.001$;
226 **, $P < 0.01$; ns, $P > 0.05$; numbers or frequencies indicate the quantities or fractions of the corresponding phenotypes; n indicates
227 the number of the analyzed individuals or cells. Scale bars, 10 µm.
228
229 **Heat tolerance of pairing and CO formation is largely lost in the progeny of Col/L*er* hybrids**
230 To further analyze the genetic underpinnings of heat tolerance of meiotic recombination, we examined homolog
231 pairing, synapsis and bivalent formation in the progeny of Col/L*er* hybrids under heat stress. Unexpectedly, in a

232 population of 1213 pachytene meiocytes from 132 Col/L*er* F2 individuals, only 11.1% of meiocytes showed full-pairing
233 of homologs. Partial-pairing and no pairing of homologs occurred 36.7% and 52.2%, respectively (Fig 5a and b).
234 Furthermore, only 19.8% of analyzed meiocytes (n = 3391) had five bivalents whereas 45.8% of meiocytes showed ten
235 univalents, with the remaining 35% having either four, three, two or one bivalents occurring at roughly similar levels
236 (Fig 5a and c). Accordingly, 48.4% of F2 individuals (n = 155) showed an average of at most one bivalent per meiocyte,
237 while 18.7% of F2 individuals showed an average of more than four bivalents per meiocyte (Fig 5d). These data
238 indicated that, in the context of bivalent formation, around half of the Col/L*er* F2 individuals behaved like Col, while
239 only about 20.0% individuals displayed a L*er*-like resistance pattern under heat stress.
240
241 We analyzed the correlation of the impact of heat on pairing, bivalent formation, and homolog segregation in the heat-
242 stressed Col/L*er* F2 population by performing Spearman's rank correlation tests using the frequencies of meiocytes
243 showing different phenotypes (Fig 5e). As expected, a strong and positive correlation was found between the numbers
244 of bivalents and homolog pairing (Fig 5e), with the presence of two, three or four bivalents per meiocyte being
245 positively correlated with the partial-pairing phenotype (Fig 5e). This correlation offered a proof that our assay system
246 worked. Moreover, positive correlations were found between balanced homolog segregation and bivalent formation
247 or successful pairing (Fig 5e). Similar correlation patterns occurred in heat-stressed inbreds and F1 hybrids (Fig S3).
248 These findings suggested that DSB formation and/or early stages of DSB repair-mediated homolog pairing are possibly
249 the primary targets of heat.
250

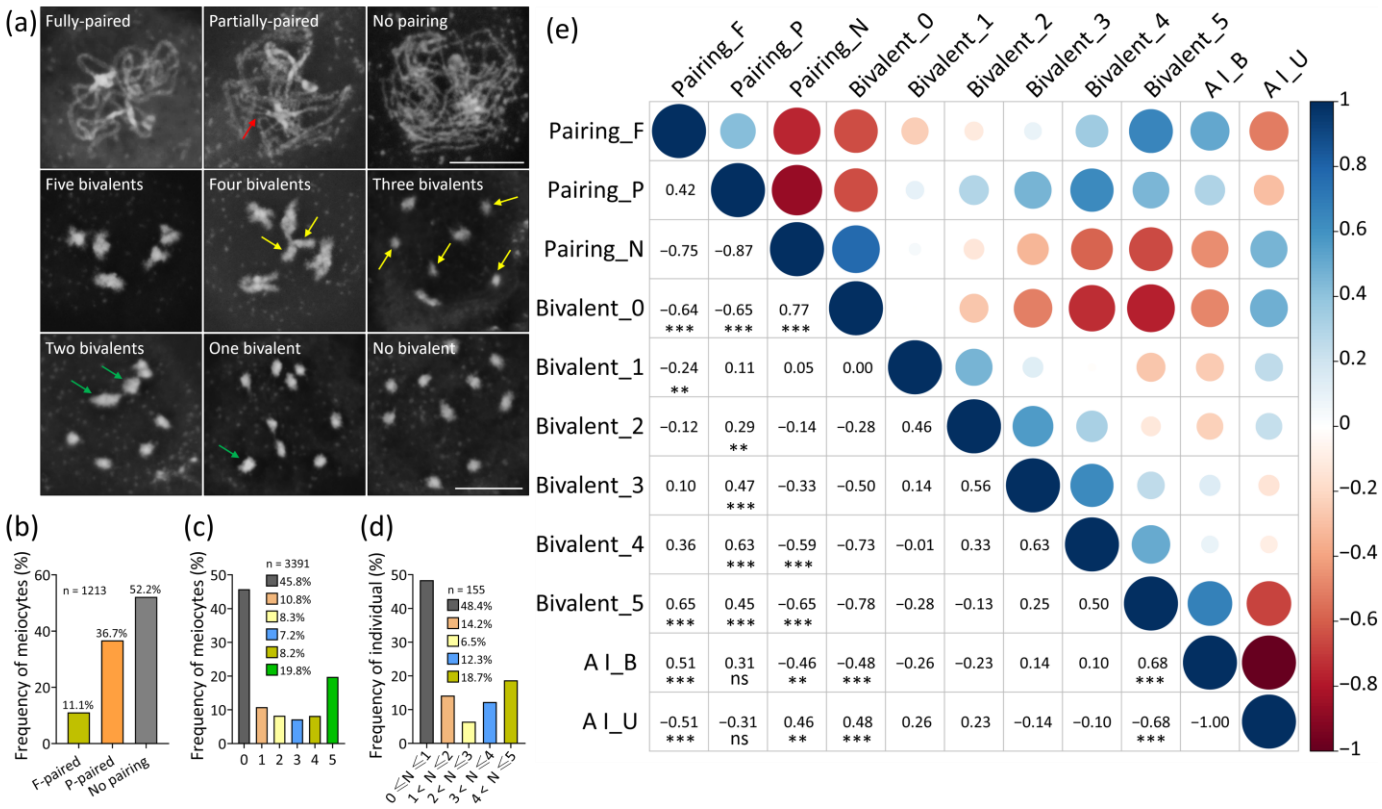

Figure 5. Chromosome pairing and bivalent formation in Col/L*er* F2 population under heat stress. (a) Representative images of chromosomes in pachytene and diakinesis showing different phenotypes of homolog pairing and bivalent formation in Col/L*er* F2 population under heat stress. The red, yellow and green arrows indicate unpaired or unsynapsed regions, univalents and bivalents, respectively. Scale bars, 10 µm. (b) Graph showing the fraction of pachytene meiocytes showing different pairing status in the heat-stressed Col/L*er* F2 population. (c) Graph showing the fraction of diakinesis meiocytes showing different numbers of bivalents in the heat-stressed Col/L*er* F2 population. (d) Graph showing the fraction of individuals in heat-stressed Col/L*er* F2 population showing different average numbers of bivalents. The frequencies indicate the rates of the corresponding phenotypes; n indicates the numbers of meiocytes or individuals; N indicates the average numbers of bivalent per meiocyte. (e) Graph showing correlation between pairing, average number of bivalents per meiocyte, and homolog segregation. Spearman correlation analysis was performed; numbers indicate the correlation coefficients between the corresponding phenotypes; significance levels of correlation were determined based on *t*-tests; ***, $P < 0.001$; **, $P < 0.01$; ns, $P > 0.05$; the significance levels in the cells without indication of significance values were not calculated.

264

265 **Heat stress reveals different impacts on chromosome morphology in interkinesis between Col and L*er* inbreds and**

266 **their F2 offspring**

267 At the end of meiosis I, homologs temporally decondense at interkinesis and then recondense at metaphase II (Fig S4).

268 We found that heat induced a less-condensed or non-condensed chromosome configuration in interkinesis, which also

269 varied between Col and L*er* (Fig 6a and c). The chromosomes exhibiting either kind of alterations in condensation

270 showed a lower DAPI fluorescence intensity compared with the ones displaying normal condensation (Fig 6a and b).

271 At 37°C, 25.0% Col plants produced meiocytes with a less-condensed chromosome configuration, while, this

272 phenotype was not observed in any analyzed L*er* plant individuals (Fig 6c). Meanwhile, meiocytes showing a non-

273 condensed chromosome configuration were observed in both Col and L*er* under heat stress (Fig 6c). Both kinds of

274 abnormalities were observed in Col/L*er* hybrids and F2 population (Fig 6c). However, in the F2 offspring that displayed

275 altered chromosome morphology, the fraction of meiocytes displaying non-condensed chromosomes was similar to

276 that in Col but higher than those in L*er* and Col/L*er* hybrids (Fig 6d), while the fraction of meiocytes exhibiting the less-

277 condensed phenotype was higher than those in inbreds and hybrids (Fig 6e).

278

279 Interestingly, positive correlations were found between the less-condensed phenotype and impaired pairing or

280 formation of only a single bivalent per meiocyte (Fig 6f and g). In addition, normal morphology of interkinesis

281 chromosomes was highly correlated with the presence of five bivalents per meiocyte (Fig 6g). The non-condensed

282 phenotype was positively associated with compromised pairing and reduced bivalent formation (Fig 6f and g). Taken

283 together, these findings implied that the loci controlling heat tolerance of homolog pairing and/or CO formation may

284 have a potential role in regulating chromosome morphology in interkinesis under heat stress.

285

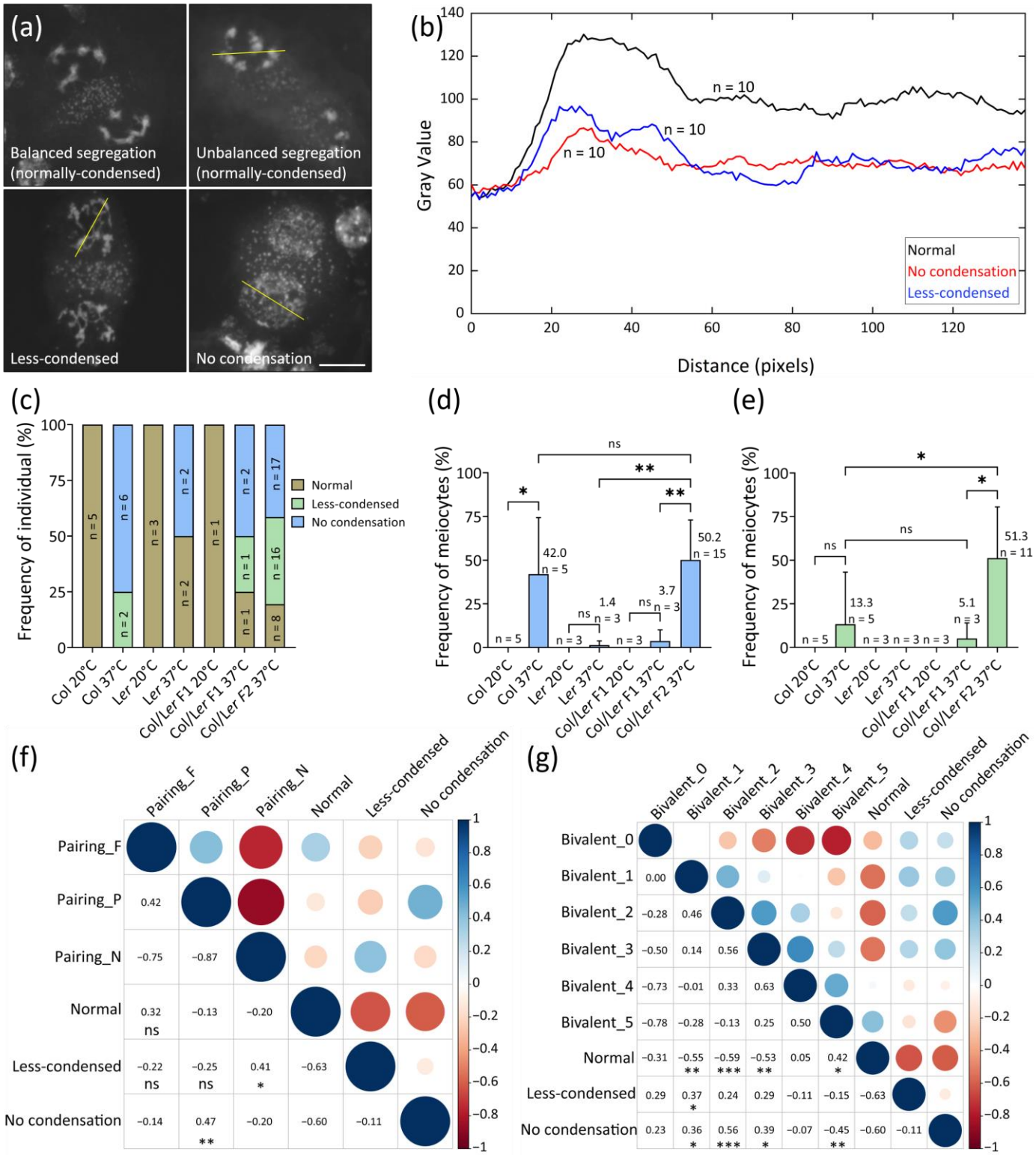

Figure 6. The impact of heat on chromosome morphology in interkinesis. (a) Representative images of different chromosome morphologies in interkinesis. Scale bar, 10 µm. (b) Average pixel intensity quantified in interkinesis meiocytes showing either kind of chromosome configuration of a section going through the middle of chromosomes (yellow lines). (c) Graph showing the rates

290 of individuals with less-condensed or non-condensed phenotypes in Col, L*er*, Col/L*er* hybrids and Col/L*er* F2 at 20°C or 37°C. n
291 indicates the numbers of plant individuals. (d and e) Graphs showing the rates of meiocytes showing non-condensed (d) or less-
292 condensed (e) phenotypes in Col, L*er*, Col/L*er* hybrids and Col/L*er* F2 at 20°C or 37°C. Stars indicate significance levels based on
293 unpaired *t* tests; n indicates the numbers of plant individuals; frequencies indicate the rates of the corresponding phenotypes. (f)
294 and (g) Graphs showing the correlation between pairing (f) and average number of bivalents per meiocyte (g) with the less-
295 condensed or non-condensed phenotypes. Spearman correlation analysis was performed; numbers indicate the correlation
296 coefficients between the corresponding phenotypes; stars indicate significance levels based on unpaired *t* tests; ***, $P < 0.001$;
297 **, $P < 0.01$; *, $P < 0.05$; ns, $P > 0.05$; the significance levels in the cells without indication of significance values were not calculated.
298

299 **Heat stress induces high levels of chromosome instabilities in the Col/L*er* F2 population**

300 Heat did not significantly increase the fraction of individuals exhibiting premature segregation of sister chromatids in
301 Col and L*er* (Fig 7a-d). In the Col/L*er* F2 population, however, 56.7% of individuals (n = 164) showed ectopic segregation
302 of sister chromatids from diakinesis to metaphase II (Fig 7b and c), suggesting that sister-chromatid cohesion was
303 perturbed. In these defect-harboring F2 plants, the fraction of meiocytes showing untimely segregation of sister
304 chromatids was significantly higher than in parental genotypes (Fig 7d). While we did not observe obvious defects in
305 chromosome integrity in Col and L*er* under heat stress, 27.0% of individuals (n = 126) in the heat-stressed Col/L*er* F2
306 population produced chromosome fragments at metaphase I, anaphase I or metaphase II (Fig 7e-g), suggesting that
307 DSB repair was defective in those F2 individuals under heat stress. Moreover, the average number of fragments per
308 meiocyte in those F2 individuals was higher than in the inbreds and hybrids (Fig 7g). These data suggested that heat
309 tolerance of chromosome stability maintenance is affected in the Col/L*er* F2 population.
310

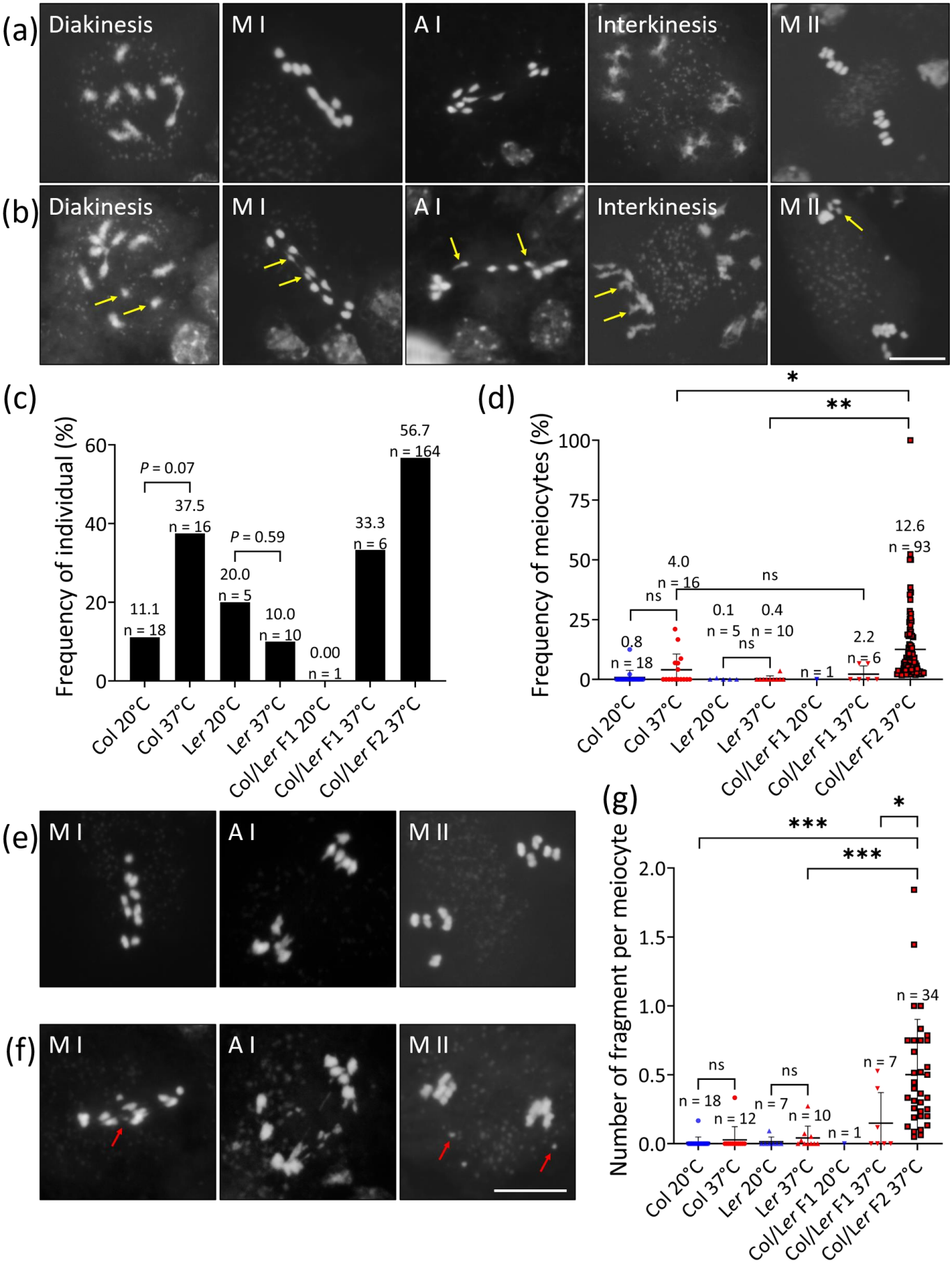
(a)
Diakinesis
M I
A I
Interkinesis
M II
(b)
Diakinesis
M I
A I
Interkinesis
M II
(c)
Frequency of individual (%)
60
40
20
0
P = 0.07
P = 0.59
11.1
n = 18
37.5
n = 16
20.0
n = 5
10.0
n = 10
0.00
n = 1
33.3
n = 6
56.7
n = 164
Col 20°C
Col 37°C
Ler 20°C
Ler 37°C
Col/Ler F1 20°C
Col/Ler F1 37°C
Col/Ler F2 37°C
(d)
Frequency of meiocytes (%)
100
75
50
25
0
*
**
ns
ns
ns
0.8
n = 18
4.0
n = 16
0.1
n = 5
0.4
n = 10
n = 1
2.2
n = 6
12.6
n = 93
Col 20°C
Col 37°C
Ler 20°C
Ler 37°C
Col/Ler F1 20°C
Col/Ler F1 37°C
Col/Ler F2 37°C
(e)
M I
A I
M II
(f)
M I
A I
M II
(g)
Number of fragment per meiocyte
2.0
1.5
1.0
0.5
0.0
***
***
*
ns
ns
n = 18
n = 12
n = 7
n = 10
n = 1
n = 7
n = 34
Col 20°C
Col 37°C
Ler 20°C
Ler 37°C
Col/Ler F1 20°C
Col/Ler F1 37°C
Col/Ler F2 37°C

311

312 Figure 7. The Col/L*er* F2 population shows a higher level of chromosome instability under heat stress. (a) and (b) Representative
313 images of diakinesis, metaphase I, anaphase I, interkinesis and metaphase II meiocytes showing normal (a) or pre-mature
314 segregation of sister chromatids (b) under heat stress. The yellow arrows indicate separated sister chromatids. (c) Graph showing
315 the rates of individuals that show abnormal segregation of sister chromatids in Col, L*er*, Col/L*er* hybrids and Col/L*er* F2 at 20°C or
316 37°C. The indicated significance levels were determined based on χ^2-tests. (d) Graph showing the rates of meiocytes exhibiting
317 premature separation of sister chromatids in Col, L*er*, Col/L*er* hybrids and Col/L*er* F2 at 20°C or 37°C. (e and f) Representative
318 images of metaphase I, anaphase I and metaphase II chromosomes with normal (e) or interfered integrity (f) under heat stress.
319 The red arrows indicate chromosome fragments. (g) Graph showing the average numbers of chromosome fragment per meiocyte
320 in Col, L*er*, Col/L*er* hybrids and Col/L*er* F2 at 20°C or 37°C. Stars indicate significance levels based on unpaired *t* tests; frequencies
321 indicate the rates of the corresponding phenotypes; n indicates the number of individuals; ***, $P < 0.001$; **, $P < 0.01$; *, $P < 0.05$;
322 ns, $P > 0.05$; scale bars, 10 µm.
323
324 **Homolog pairing and synapsis facilitate timely sister-chromatids separation under heat stress**
325 We then related homolog pairing and bivalent formation with the phenotype of premature sister-chromatids
326 separation in our heat-stressed Col/L*er* F2 population. A positive but weak correlation was detected between the
327 fraction of meiocytes showing cohesion defect with the fraction of meiocytes showing partial pairing, or the diakinesis
328 meiocytes producing an average of one bivalent (Fig 8a and b). Notably, among the meiocytes showing ectopic sister-
329 chromatid separation, the meiocytes in metaphase I, anaphase I or metaphase II stages occupied 8.7%, 35.8% and
330 59.0%, respectively (Fig 8c). This implied that heat stress primarily destabilizes centromeric cohesion in late or after
331 meiosis I. Moreover, we found a strong and positive correlation between the fraction of meiocytes exhibiting
332 chromosome fragmentations with meiocytes in pachytene undergoing normal homolog pairing (Fig 8d) and with
333 meiocytes in diakinesis producing five bivalents (Fig 8e).

334

335 To further investigate the impact of homolog pairing and/or synapsis and CO formation on sister-chromatids cohesion
336 under heat stress, we analyzed a *spo11-1* mutant (Col background), in which DSB formation is largely abolished and
337 homolog pairing and recombination are impaired (56). Untimely separation of sister chromatids was observed in
338 *spo11-1* at both temperatures, but there was no significant difference (Fig 8f-h, $P > 0.05$). Next, we analyzed the *dmc1*
339 (Col background), in which DSBs are formed but homolog pairing and CO formation do not occur (57), and the double
340 *zyp1a*/*b* mutant (Col background), in which homolog pairing occurs but synapsis is impaired (14, 58, 59). Both *dmc1*
341 and *zyp1a*/*b* exhibited premature sister-chromatids segregation at 20°C, and, the fraction of meiocytes showing the
342 cohesion defect in both mutants were significantly increased under heat stress (Fig 8f-h; $P < 0.01$ for *dmc1* and $P <$
343 0.001 for *zyp1a*/*b*). Interestingly, the defect-harboring meiocytes in *dmc1* occurred by 66.7% at and/or prior to
344 anaphase I, while, in *zyp1a*/*b*, the irregularity was found by 79.2% at metaphase II (Fig 8i). These findings implied that
345 DMC1- and ZYP1-dependent homolog pairing and/or synapsis play a role in facilitating timely separation of sister
346 chromatids under heat stress, yet possibly via different mechanisms. To address if the distinct distribution of
347 differently-staged meiocytes showing ectopic sister-chromatids separation between *dmc1* and *zyp1a*/*b* was owing to
348 the difference in CO formation, we examined a *msh4* mutant (Col background), which undergoes normal homolog
349 synapsis but loses approximately 85% COs (60). No significant difference in the rates of meiocytes with cohesion defect
350 was detected at 20°C and 37°C (Fig 8h, $P > 0.05$).

351

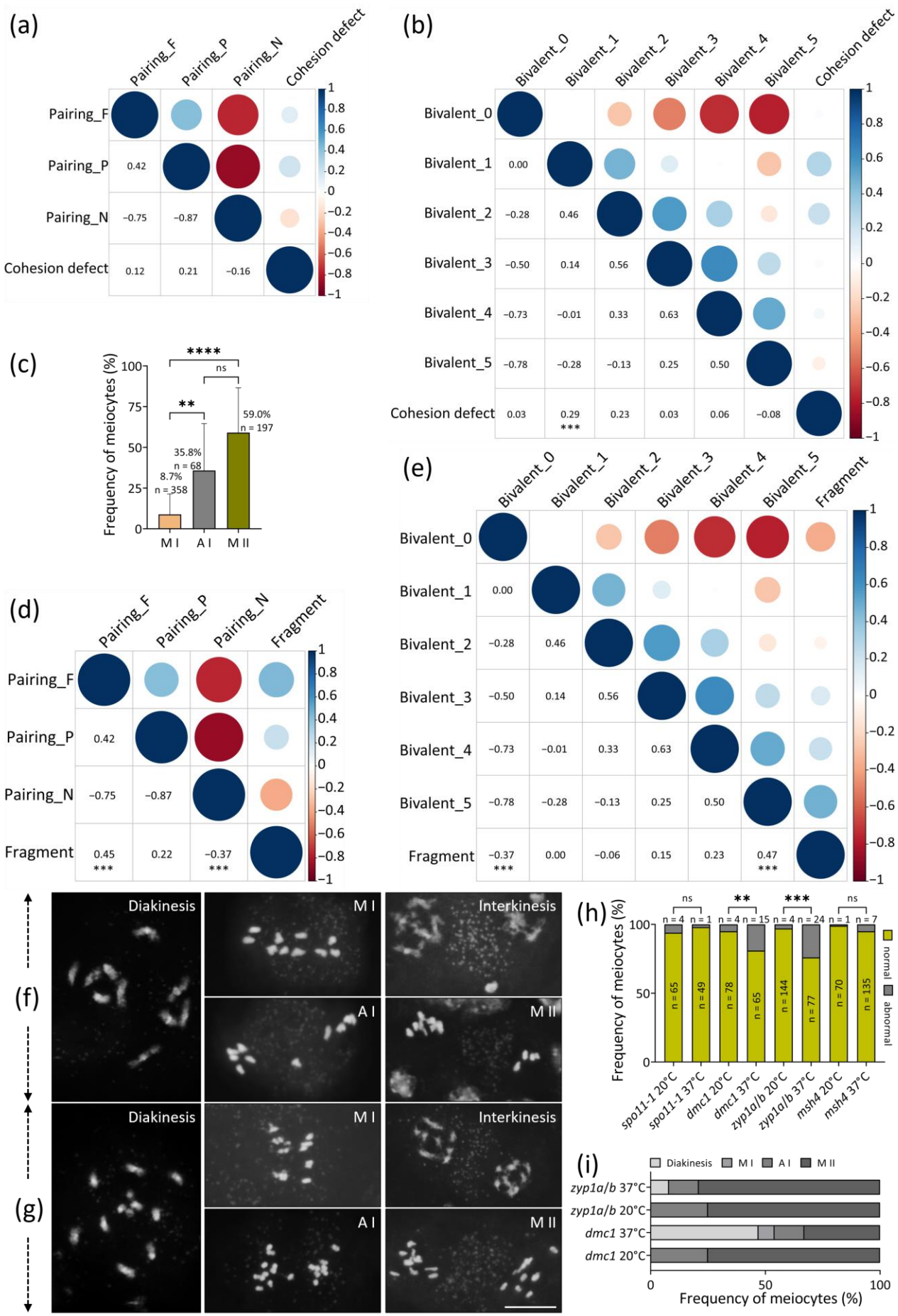
(a)
Pairing_F
Pairing_P
Pairing_N
Cohesion defect
0.42
−0.75
−0.87
0.12
0.21
−0.16
(b)
Bivalent_0
Bivalent_1
Bivalent_2
Bivalent_3
Bivalent_4
Bivalent_5
Cohesion defect
0.00
−0.28
0.46
−0.50
0.14
0.56
−0.73
−0.01
0.33
0.63
−0.78
−0.28
−0.13
0.25
0.50
0.03
0.29
***
0.23
0.03
0.06
−0.08
(c)
Frequency of meiocytes (%)
****
ns
**
59.0%
n = 197
35.8%
n = 68
8.7%
n = 358
M I
A I
M II
(d)
Pairing_F
Pairing_P
Pairing_N
Fragment
0.42
−0.75
−0.87
0.45
***
0.22
−0.37
***
(e)
Bivalent_0
Bivalent_1
Bivalent_2
Bivalent_3
Bivalent_4
Bivalent_5
Fragment
0.00
−0.28
0.46
−0.50
0.14
0.56
−0.73
−0.01
0.33
0.63
−0.78
−0.28
−0.13
0.25
0.50
−0.37
***
0.00
−0.06
0.15
0.23
0.47
***
(f)
Diakinesis
M I
Interkinesis
A I
M II
(g)
Diakinesis
M I
Interkinesis
A I
M II
(h)
Frequency of meiocytes (%)
ns
**
***
ns
n = 4
n = 1
n = 4
n = 15
n = 4
n = 24
n = 1
n = 7
n = 65
n = 49
n = 78
n = 65
n = 144
n = 77
n = 70
n = 135
normal
abnormal
spo11-1 20°C
spo11-1 37°C
dmc1 20°C
dmc1 37°C
zyp1a/b 20°C
zyp1a/b 37°C
msh4 20°C
msh4 37°C
(i)
Diakinesis
M I
A I
M II
zyp1a/b 37°C
zyp1a/b 20°C
dmc1 37°C
dmc1 20°C
Frequency of meiocytes (%)

352

353 Figure 8. Homolog pairing and synapsis facilitate timely sister-chromatids separation under heat stress. (a and b) Graphs showing
354 the correlation between the rates of meiocytes showing different pairing status (a) or bivalent formation (b) with the frequency
355 of meiocytes with cohesion defect in the Col/L*er* F2 population under heat stress. (c) Graph showing the rates of metaphase I,
356 anaphase I and metaphase II meiocytes with cohesion defect in the Col/L*er* F2 population under heat stress. (d and e) Graphs
357 showing the correlation between the frequencies of meiocytes showing different pairing status (d) or bivalent formation (e) with
358 the rate of meiocytes showing chromosome fragmentation in the Col/L*er* F2 population under heat stress. Spearman correlation
359 analysis was performed. Numbers indicate the correlation coefficients between the corresponding phenotypes; significance of
360 correlation was calculated using *t*-tests; the significance levels in the cells without indication of significance values were not
361 calculated. (f and g) Representative images of diakinesis, metaphase I, anaphase I, interkinesis and metaphase II meiocytes
362 showing normal (f) or untimely sister-chromatids separation (g). (h) Graph showing the rates of meiocytes with normal or untimely
363 sister-chromatids separation in *spo11-1*, *dmc1*, *zyp1a/b* and *msh4* at 20°C and 37°C. (i) Graph showing the rates of different
364 meiosis-staged meiocytes exhibiting untimely sister-chromatids separation in *dmc1* and *zyp1a/b* at 20°C and 37°C. For (c) and (h),
365 χ^2-tests were performed; frequencies indicate the rates of the corresponding phenotypes; n indicates the number of analyzed
366 cells; ***, $P < 0.001$; **, $P < 0.01$; ns, $P > 0.05$; scale bar, 10 µm.
367

368 **Chromosome integrity in both Col and L*er* under heat stress relies on functional ATM**

369 We previously reported that ATM-controlled DSB repair is required for maintenance of meiotic chromosome integrity
370 in Col under heat stress (51). Thus, we decided to examine whether the role of ATM in protecting chromosome stability
371 under heat stress varies between Col and L*er*. To this end, we took advantage of an *atm* mutant allele, *atm-5*, which is
372 in L*er* background and shows defects in DSB repair (61). We found that, as the case in *atm-2*, an allele in Col background
373 (51), chromosome fragments in *atm-5* was significantly increased after heat treatment (Fig 9a and b; $P < 0.001$). A bi-
374 allelic *atm* mutant $ATM^{atm\text{-}2/atm\text{-}5}$, which harbored the *atm-2* and *atm-5* alleles on either homolog, was generated, and

375 behaved similarly as *atm-2* and *atm-5* under heat stress (Fig 9c and d). We also examined the impact of heat on
376 homolog pairing in *atm-5*. At 20°C, most pachytene meiocytes showed normal pairing and synapsis of homologs, and
377 16.9% of meiocytes showed a partial pairing phenotype (Fig 9e and g). At 37°C, most pachytene meiocytes in *atm-5*
378 showed a partial pairing phenotype, with only 3.9% cells showing an impaired homolog pairing (Fig 9e and g), similar
379 to the case in heat-stressed L*er* (Fig 3j). Immunolocalization revealed an increased level of patchy ZYP1 configuration
380 in *atm-5* compared with that in L*er* (Fig 9f and h; Fig 3t), which was likely caused by the disrupted chromosome integrity
381 due to ATM dysfunction (51). Similar alterations in homolog pairing and SC formation were observed in $ATM^{atm\text{-}2/atm\text{-}5}$
382 at either temperature (Fig 9i-l). These data suggest that there is no accession-specific difference in dependency of
383 ATM-mediated DSB repair for meiotic chromosome integrity under heat stress.
384

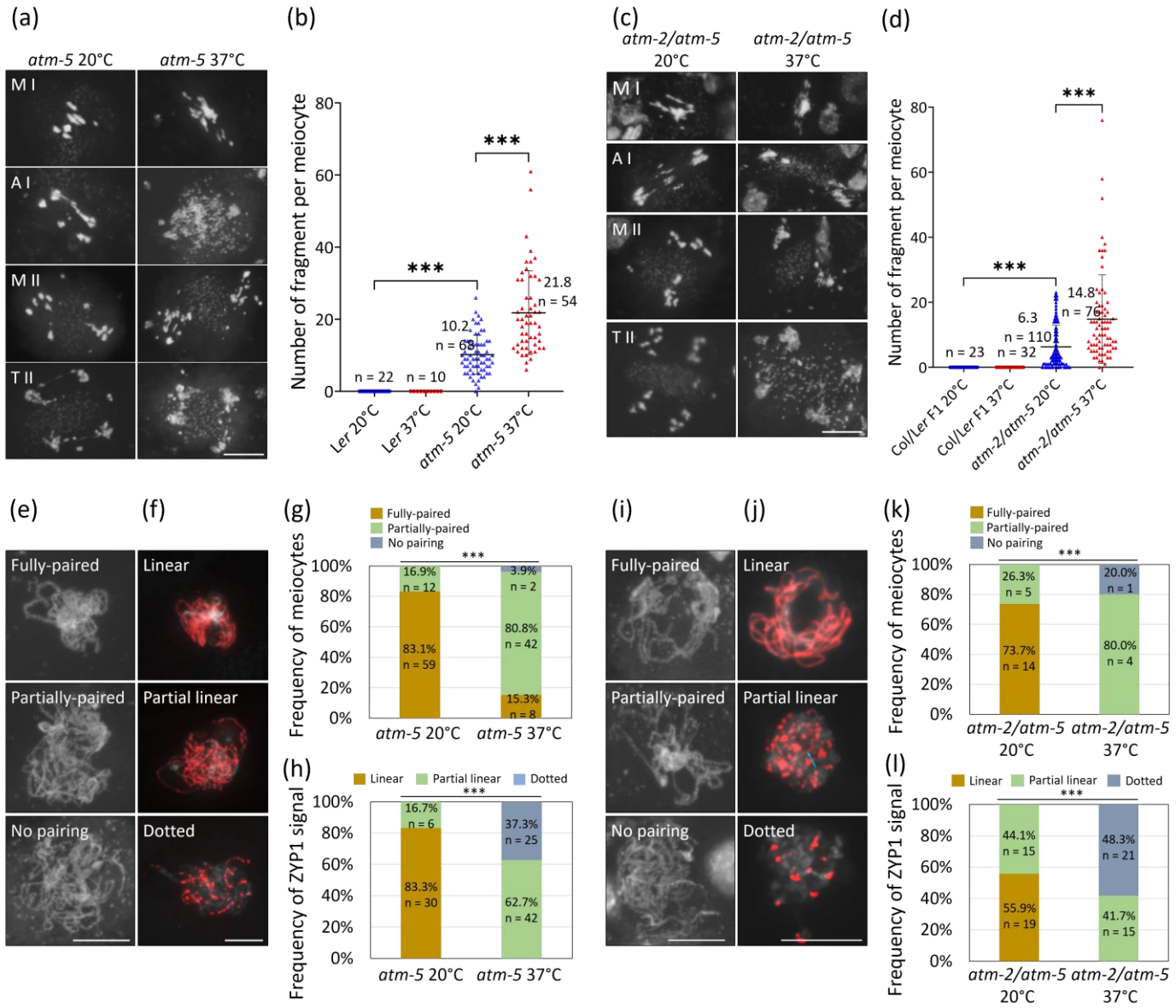

Figure 9. Chromosome integrity under heat stress in both Col and L*er* relies on ATM. (a and c), Metaphase I, anaphase I, metaphase II and telophase II chromosomes in *atm-5* (a) and *ATM*$^{atm\text{-}2/atm\text{-}5}$ (c) at 20°C and 37°C. (b and d), Graphs showing the average number of chromosome fragment in *atm-5* (b) and *ATM*$^{atm\text{-}2/atm\text{-}5}$ (d) at 20°C and 37°C. Significance levels are shown based on unpaired *t* tests. (e and i), Representative images of pachytene chromosomes showing fully-paired, partially-paired, or no pairing in *atm-5* (e) and *ATM*$^{atm\text{-}2/atm\text{-}5}$ (i) at 20°C and 37°C. (f and j), Representative images of immunolocalization of ZYP1 on pachytene chromosomes showing linear, partial linear, or patchy phenotypes in *atm-5* (f) and *ATM*$^{atm\text{-}2/atm\text{-}5}$ (j) at 20°C and 37°C. The blue arrow indicates linear ZYP1 signals. (g and k), Graphs showing the rates of different pairing status of pachytene chromosomes in *atm-5* (g) and *ATM*$^{atm\text{-}2/atm\text{-}5}$ (k) at 20°C and 37°C. Significance levels are shown based on χ^2-tests. (h and l), Graphs showing the rates of different

394 ZYP1 configurations on pachytene chromosomes in *atm-5* (h) and *ATM*$^{atm-2/atm-5}$ (l) at 20°C and 37°C. Significance levels are shown

395 based on χ^2-tests; frequencies or numbers indicate the rate or quantity of the corresponding phenotypes; n indicates the number

396 of analyzed cells; ***, $P < 0.001$; scale bars, 10 µm.

397

398 **Discussion**

399 Our previous study demonstrated that heat stress reduces DSB formation and disrupts pairing as well as synapsis of

400 homologs in Col (36, 37). In this study, we report that Col and L*er* have a striking difference in heat tolerance of meiotic

401 recombination. Specifically, heat stress does not impair SC formation and does not reduce the numbers of RAD51 or

402 DMC1 foci in L*er* (Fig 2 and 3). Based on our previous studies, the distinct heat tolerance of DSB formation between

403 Col and L*er* is likely due to a difference in the activity and/or localization of the recombination proteins, and not in

404 transcription levels (36, 51). Since the number of bivalents is strongly correlated with homolog pairing status (Fig 5), it

405 is likely that heat suppresses meiotic recombination predominantly by interfering with DSB formation and/or the

406 RAD51- and DMC1-mediated homolog pairing. In support, DMC1 has been found to play a role in maintaining CO

407 formation at high temperature in wheat (62, 63). Nevertheless, since there is still a low level of DSBs in heat-stressed

408 Col (Fig 2), and some meiocytes in L*er* display compromised homolog pairing under heat stress (Fig 3), we propose

409 that heat can also directly attenuate homolog pairing apart from reducing DSB formation (36, 37, 51, 64). Based on

410 the analysis of Col/L*er* hybrids, we conclude that the heat tolerance of meiotic recombination in L*er* is a dominant trait

411 (Fig 4). 10% ~ 20% of F2 offspring behaving as L*er* suggests that the dominance relies on the presence of several alleles.

412 While all alleles are present in Col/L*er* hybrids, the linkage of these alleles is broken in the meiosis of these hybrids

413 leading to a differentiated pattern of heat tolerance in the F2 population (Fig 5).

414

415 Heat induces an increased fraction of interkinesis meiocytes displaying a non-condensed chromosome configuration

416 in Col, which does not occur in L*er* and the Col/L*er* F1 hybrids, but occurs again, and, at the same level, in the F2
417 population (Fig 6d). Meanwhile, heat increases the rate of interkinesis meiocytes exhibiting a less-condensed
418 phenotype in some F2 individuals but not in inbreds or hybrids, which suggests a higher heat sensitivity in F2 offspring
419 (Fig 6e). The heat-induced abnormalities in interkinesis phenotypically mimic slowed meiosis progression or a failure
420 of entering into meiosis II, which implies that meiosis progression and/or cell cycle transition may be perturbed
421 possibly due to alterations in expression and/or function of *TAM/CYCA1;2* (*TAM*) or *OMISSION OF SECOND DIVISION 1*
422 (*OSD1*), or other meiotic cell cycle regulators (36, 65-67). Furthermore, correlation analysis suggests that meiotic
423 recombination or its related regulators may impact meiotic cell cycle progression and/or chromosome morphology
424 after anaphase I beyond its impact on prophase I progression under heat stress (Fig 6) (25).
425
426 Incorrect sister-chromatids separation in the F2 offspring (Fig 7) implies that heat perturbs the function of the cohesion
427 complex. It has recently been reported that high temperatures reduce the amounts of CENH3 in Arabidopsis (35),
428 which may lead to interfered centromere function and cohesion instability. Notably, we found that most meiocytes
429 showing cohesion defects are in anaphase I or metaphase II (Fig 8), suggesting that heat primarily perturbs centromeric
430 cohesion during anaphase I and interkinesis. In Arabidopsis, SHUGOSHIN 1 (SGO1) and PROTEIN PHOSPHATASE 2A
431 (PP2A), and the Arabidopsis homolog of securin PATRONUS (PANS1) protect meiotic centromeric cohesion at anaphase
432 I and diakinesis, respectively (68-71). In addition, PP2A is co-expressed with genes involved in response to abiotic
433 stresses including heat in multiple developmental stages in Arabidopsis (72). It is thus possible that heat stress alters
434 the expression and/or function of these cohesion regulators. In multiple species, bivalent formation is required for
435 correct orientation of sister kinetochores and thus balanced chromosome segregation in meiosis I (73-78). Our
436 correlation analysis suggests that homolog pairing and/or synapsis but possibly not chiasmata formation may directly
437 or indirectly impact timely sister-chromatids separation under heat stress (Fig 8). However, heat-stressed *spo11-1* does

438 not show a higher level of defective sister-chromatids separation (Fig 8), suggesting that the effect of heat stress on
439 homolog pairing-mediated cohesion stability may rely on DSB formation, and, the increased aneuploid nuclei due to
440 chromosome mis-segregation observed in heat-stressed *spo11-2* are not owing to premature sister-chromatids
441 separation (35).
442
443 We observed an increase of chromosome fragments in some Col/L*er* F2 individuals but not in either inbreds or hybrids
444 under heat stress (Fig 7), suggesting that DSB repair is perturbed in those fragment-harboring F2 plants. This
445 phenotype, together with the increased fraction of meiocytes showing premature sister-chromatid separation, imply
446 that transgressive effects become visible in the F2 population showing defects exceeding that observed in parents.
447 ATM-mediated DSB repair is required for meiotic chromosome integrity in both Col and L*er* under heat stress (Fig 9)
448 (51), dysfunction of which might be one of the mechanisms that underpin the heat-interfered chromosome integrity
449 in those F2 individuals. The upstream factor and/or signaling pathway that regulates ATM expression or activity in DSB
450 repair in response to heat stress require further investigation. Our data suggest that there is no accession-specific
451 difference in the dependency of ATM-mediated DSB repair for maintenance of meiotic chromosome integrity under
452 heat stress. Alternatively, ATM-mediated mechanism acts in an epistatic manner to protect meiotic chromosome
453 stability under heat stress. Interestingly, the fragmentation phenotype is strongly and positively correlated with
454 successful homolog pairing and bivalent formation (Fig 8d and e). We speculate that these associations are possibly a
455 subsequent effect of heat stress on DSB formation and repair, the heat tolerance of which are regulated via different
456 pathways. Specifically, in the individuals that show normal homolog pairing and CO formation, DSB formation likely
457 occurs normally, however, DSB repair may be perturbed, which consequently leads to lesions in chromosome integrity.
458 On the contrary, the individuals with impaired homolog pairing and CO formation likely have a significantly reduced
459 DSB formation, which compensates for the perturbation of DSB repair, and thus show relatively undisturbed

460 chromosome integrity. Thus, DSB formation and homolog pairing likely are the predominant targets, which facilitate
461 meiosis progression and genome stability at post-recombination stages under heat stress. Taken together, our study
462 reveals that natural variation in multiple genomic loci controls heat tolerance of meiosis in Arabidopsis, holding a great
463 potential to be exploited in breeding programs.
464

465 ## Material and Methods

466 **Plant materials and growth conditions**

467 *Arabidopsis thaliana* (L.) accessions Columbia-0 (Col-0) and Landsberg *erecta* (L*er*), the *atm-2* (50), *atm-5* (61), *er-105*,
468 *mpk6*, *er-105 mpk6* (52), *dmc1* (79), *spo11-1-3* (56), *msh4* (60) and *zyp1a/b* (14) mutants were used in this study. For
469 simplification 'Col' was used throughout the main text. Col/L*er* hybrids were obtained by crossing using L*er* as pollen
470 donator. The bi-allelic mutant $ATM^{atm\text{-}2/atm\text{-}5}$ was obtained by crossing the heterozygous *atm-2* and *atm-5* mutants.
471 Genotyping was performed using the primers listed in Table S1. Arabidopsis were cultivated in a growth chamber with
472 a 16 h day/8 h night and 20°C condition. For heat treatment, young flowering plants were treated by 37°C for 24 h in
473 a humid chamber with a 16 h day/8 h night condition. To avoid potential impact of circadian clock, heat treatment was
474 applied starting from 8:00-10:00 am.
475

476 **Cytological analysis of meiocytes**

477 After heat treatment, plants were transferred back to 20°C for 6-12 h recovery, and tetrad stage meiocytes were
478 analyzed (38). A drop of 4.5% (w/v) lactopropionic orcein staining buffer was added to the surface of a tetrad-staged
479 flower bud (floral bud stage 9, 0.3-0.4 mm) (80) followed by squashing to release meiocytes.
480

481 **Preparation of chromosome spreads**

482 Inflorescences were isolated and fixed in cold Carnoy's fixative for at least 24 h. Flower buds at stages beyond tetrads
483 were removed, and the remaining buds were washed twice in distilled water and once in citrate buffer (10 mM, pH =
484 4.5), followed by incubation in a digestion enzyme mixture (0.3% pectolyase and 0.3% cellulase in citrate buffer) at
485 37°C for 3 h. Digested flower buds were subsequently washed once in distilled water, which thereafter were macerated
486 in distilled water on a glass slide. Two rounds of 60% acetic acid were added to the slide, which was dried on a hotplate
487 at 45°C. The slide was flooded with cold Carnoy's fixative and then was air dried. 4',6-diamidino-2-phenylindole (DAPI)
488 was diluted to 5 μg/mL in Vectashield antifade mounting media (Vector Laboratories).
489

490 **Immunolocalization of α-tubulin and meiotic recombination proteins**

491 To perform immunolocalization of α-tubulin, inflorescences were fixed by 4% (w/v) paraformaldehyde under vacuum
492 for 30 min, followed by twice washes in distilled water and once in citrate buffer (10 mM, pH = 6.0). Meiosis-staged
493 flower buds were digested in an enzyme mixture consisting of 0.3% (w/v) cellulase (Sigma), 0.3% (w/v) pectolyase
494 (Sigma) and 0.3% (w/v) cytohelicase (Sigma) in a humid chamber at 37°C for 3 h. After the digestion, anthers were
495 dissected, squashed, and fixed on a slide by freezing in liquid nitrogen. Released cells on the slide were immobilized
496 with a thin layer of gel containing 1% (w/v) gelatin, 1% (w/v) agarose and 2.5% (w/v) sucrose. After rinsing with
497 phosphate buffered saline with 1% (v/v) Triton-X 100 for 30 min, the α-tubulin antibody diluted in phosphate buffered
498 saline with 0.1% (v/v) Triton X-100 and 4.5 g/L bovine serum albumin was added and the slide was incubated overnight
499 at 4°C. The slide washed three times with phosphate buffered saline with 0.02% tween-20 was incubated with a
500 secondary antibody at 37°C for 1 h in the dark. Immunolocalization of meiotic recombination proteins was performed
501 as previously described (81, 82), and the antibodies used in this study have been reported previously (36, 38, 51).
502

503 **Quantification of fluorescent foci, fluorescence intensity and chromosome fragments**

504 Fluorescent images were taken by an Olympus IX83 inverted fluorescence microscope with a X-Cite lamp and a Prime
505 BSI camera, and Z-stacks were processed using ImageJ. The fluorescent foci merged onto DAPI-stained chromosomes
506 were counted. For the pixel intensity plot, the pixel brightness through a region of interest was measured using ImageJ
507 and plotted against the X dimension. To score the number of chromosome fragments, chromosome bodies in
508 meiocytes at metaphase I, anaphase I and metaphase II that were obviously brighter than organelles were counted
509 followed by a subtraction of expected chromosome number (5 at metaphase I, 10 at anaphase I or metaphase II).
510

511 **Statistical analysis**

512 Significance was calculated using unpaired *t*-tests (Fig 1b; Fig 2c, d, h and j; Fig 4b, d, and h; Fig 6d and e; Fig 7d and g;
513 Fig 9b and d) or Chi-squared tests (Fig 1f; Fig 2f; Fig 3j, l and t; Fig 4f, j, l and n; Fig 7c; Fig 8c and h; Fig 9g, h, k and l)
514 with the software GraphPad Prism. The significance level was set as $P < 0.05$. To calculate the frequency of individuals
515 or meiocytes showing either altered chromosome morphology in interkinesis (Fig 6c, d and e), untimely sister-
516 chromatids segregation, or number of chromosome fragments (Fig 7c, d and g), the individuals, in which a meiocyte
517 with the corresponding defect was observed, and at least three meiocytes at the corresponding stage were found,
518 were used for calculation. The numbers of analyzed meiocytes or individuals are shown in the figures or main text.
519 Correlation between different meiosis phenotypes was determined based on Spearman's rank correlation tests.
520 Coefficients were calculated using Corrplot package on the R statistical platform, and Ggpubr package was used for
521 visualization.
522

523 **Acknowledgement**

524 The authors thank the National Natural Science Foundation of China (32000245), Hubei Provincial Natural Science
525 Foundation of China (2024AFB695), the Fundamental Research Funds for the Central Universities of South-Central

Minzu University (CZZ24011), Knowledge Innovation Program of Wuhan-Shuguang Project (2022020801020410) and general funds of University of Hamburg (to A.S.) for the financial support on this study. They thank Pingli Lu (Henan University) for sharing the *atm-5* mutants. They thank Chao Yang (HZAU) for providing the *zyp1a/b* mutant. They thank Yuan Qin (FAFU) for sharing the *er-105*, *mpk6* and the *er-105 mpk6* mutants.

Author contributions

Conceptualization: Bing Liu.

Data curation: Jiayi Zhao, Bing Liu.

Formal analysis: Jiayi Zhao, Zhengze Wang, Ziming Ren, Zhihua Wu and Xiaoning Lei.

Funding acquisition: Arp Schnittger, Bing Liu.

Investigation: Jiayi Zhao, Huiqi Fu, Min Zhang, Yaoqiong Liang, Xueying Cui, Wenjing Pan, Yujie Zhang, Xin Gui, Li Huo, Chong Wang.

Methodology: Jiayi Zhao, Arp Schnittger, Wojciech P. Pawlowski, Bing Liu.

Project administration: Bing Liu.

Resources: Bing Liu.

Supervision: Bing Liu.

Validation: Jiayi Zhao, Bing Liu.

Writing - original draft: Bing Liu.

Writing - review & editing: Jiayi Zhao, Huiqi Fu, Arp Schnittger, Wojciech P. Pawlowski, Bing Liu.

Data availability

All data supporting the conclusions drawn in our study are fully documented in this article and Supporting Information

548 (including Fig S1–S4; Table S1).

549

550 **Accession numbers**

551 Accession numbers of genes studied in this work are: *SPO11-1* (AT3G13170), *RAD51* (AT5G20850), *DMC1* (AT3G22880),

552 *ASY4* (AT2G33793), *ZYP1A* (AT1G22260), *ZYP1B* (AT1G22275), *HEI10* (AT1G53490), *ERECTA* (AT2G26330), *MPK6*

553 (AT2G43790), *ATM* (AT3G48190) and *MSH4* (AT4G17380).

554

555 **References**

556 1. Vrielynck N, Schneider K, Rodriguez M, Sims J, Chambon A, Hurel A, et al. Conservation and divergence of meiotic DNA double
557 strand break forming mechanisms in Arabidopsis thaliana. Nucleic Acids Res. 2021;49(17):9821-35.
558 2. Nore A, Juarez-Martinez AB, Clément J, Brun C, Diagouraga B, Laroussi H, et al. TOPOVIBL-REC114 interaction regulates
559 meiotic DNA double-strand breaks. Nat Commun. 2022;13(1):7048.
560 3. Chen H, He C, Wang C, Wang X, Ruan F, Yan J, et al. RAD51 supports DMC1 by inhibiting the SMC5/6 complex during meiosis.
561 Plant Cell. 2021;33(8):2869-82.
562 4. Da Ines O, Degroote F, Goubely C, Amiard S, Gallego ME, White CI. Meiotic recombination in Arabidopsis is catalysed by DMC1,
563 with RAD51 playing a supporting role. Plos Genet. 2013;9(9):e1003787.
564 5. Kurzbauer MT, Uanschou C, Chen D, Schlogelhofer P. The recombinases DMC1 and RAD51 are functionally and spatially
565 separated during meiosis in Arabidopsis. Plant Cell. 2012;24(5):2058-70.
566 6. Su H, Cheng Z, Huang J, Lin J, Copenhaver GP, Ma H, et al. Arabidopsis RAD51, RAD51C and XRCC3 proteins form a complex
567 and facilitate RAD51 localization on chromosomes for meiotic recombination. Plos Genet. 2017;13(5):e1006827.
568 7. Ziolkowski PA. Why do plants need the ZMM crossover pathway? A snapshot of meiotic recombination from the perspective
569 of interhomolog polymorphism. Plant Reproduction. 2023;36(1):43-54.
570 8. Wang Y, Copenhaver GP. Meiotic recombination: mixing it up in plants. Annu Rev Plant Biol. 2018;69:577-609.
571 9. Jones GH, Franklin FC. Meiotic crossing-over: obligation and interference. Cell. 2006;126(2):246-8.
572 10. Armstrong SJ, Caryl AP, Jones GH, Franklin FC. Asy1, a protein required for meiotic chromosome synapsis, localizes to axis-
573 associated chromatin in Arabidopsis and Brassica. Journal of Cell Science. 2002;115(Pt 18):3645-55.
574 11. Chambon A, West A, Vezon D, Horlow C, De Muyt A, Chelysheva L, et al. Identification of ASYNAPTIC4, a component of the
575 meiotic chromosome axis. Plant Physiology. 2018;178(1):233-46.
576 12. Ferdous M, Higgins JD, Osman K, Lambing C, Roitinger E, Mechtler K, et al. Inter-homolog crossing-over and synapsis in
577 Arabidopsis meiosis are dependent on the chromosome axis protein AtASY3. Plos Genet. 2012;8(2):e1002507-e.
578 13. West AM, Rosenberg SC, Ur SN, Lehmer MK, Ye Q, Hagemann G, et al. A conserved filamentous assembly underlies the
579 structure of the meiotic chromosome axis. eLife. 2019;8.
580 14. Yang C, Sofroni K, Hamamura Y, Hu B, Elbasi HT, Balboni M, et al. ZYP1-mediated recruitment of PCH2 to the synaptonemal
581 complex remodels the chromosome axis leading to crossover restriction. Nucleic Acids Res. 2022;50(22):12924-37.
582 15. Lambing C, Tock AJ, Topp SD, Choi K, Kuo PC, Zhao X, et al. Interacting genomic landscapes of REC8-cohesin, chromatin, and
583 meiotic recombination in Arabidopsis. Plant Cell. 2020;32(4):1218-39.

584 16. Lambing C, Kuo PC, Tock AJ, Topp SD, Henderson IR. ASY1 acts as a dosage-dependent antagonist of telomere-led
585 recombination and mediates crossover interference in Arabidopsis. Proc Natl Acad Sci U S A. 2020;117(24):13647-58.
586 17. Yang C, Hamamura Y, Sofroni K, Böwer F, Stolze SC, Nakagami H, et al. SWITCH 1/DYAD is a WINGS APART-LIKE antagonist that
587 maintains sister chromatid cohesion in meiosis. Nat Commun. 2019;10(1):1755-.
588 18. Onn I, Heidinger-Pauli JM, Guacci V, Unal E, Koshland DE. Sister chromatid cohesion: a simple concept with a complex reality.
589 Annual review of cell and developmental biology. 2008;24:105-29.
590 19. Chen Y, Zhang Q, Teng Z, Liu H. Centromeric transcription maintains centromeric cohesion in human cells. Journal of Cell
591 Biology. 2021;220(7).
592 20. McKinley KL, Cheeseman IM. The molecular basis for centromere identity and function. Nature Reviews Molecular Cell
593 Biology. 2016;17(1):16-29.
594 21. Modliszewski JL, Copenhaver GP. Meiotic recombination gets stressed out: CO frequency is plastic under pressure. Current
595 Opinion in Plant Biology. 2017;36:95-102.
596 22. Bomblies K, Higgins JD, Yant L. Meiosis evolves: adaptation to external and internal environments. New Phytologist.
597 2015;208(2):306-23.
598 23. Liu B, Mo WJ, Zhang D, De Storme N, Geelen D. Cold influences male reproductive development in plants: a hazard to fertility,
599 but a window for evolution. Plant Cell Physiology. 2019;60(1):7-18.
600 24. De Jaeger-Braet J, Schnittger A. Heating up meiosis – chromosome recombination and segregation under high temperatures.
601 Current Opinion in Plant Biology. 2024;80:102548.
602 25. De Jaeger-Braet J, Krause L, Buchholz A, Schnittger A. Heat stress reveals a specialized variant of the pachytene checkpoint in
603 meiosis of Arabidopsis thaliana. Plant Cell. 2022;34(1):433-54.
604 26. De Storme N, Copenhaver GP, Geelen D. Production of diploid male gametes in Arabidopsis by cold-induced destabilization
605 of postmeiotic radial microtubule arrays. Plant Physiology. 2012;160(4):1808-26.
606 27. Liu B, De Storme N, Geelen D. Cold-induced male meiotic restitution in Arabidopsis thaliana is not mediated by GA-DELLA
607 signaling. Front Plant Sci. 2018;9:91.
608 28. Tang Z, Zhang L, Yang D, Zhao C, Zheng Y. Cold stress contributes to aberrant cytokinesis during male meiosis I in a wheat
609 thermosensitive genic male sterile line. Plant Cell and Environment. 2011;34(3):389-405.
610 29. Zhou Q, Cheng X, Kong B, Zhao Y, Li Z, Sang Y, et al. Heat shock-induced failure of meiosis I to meiosis II transition leads to 2n
611 pollen formation in a woody plant. Plant Physiology. 2022;189(4):2110-27.
612 30. De Storme N, Geelen D. High temperatures alter cross-over distribution and induce male meiotic restitution in Arabidopsis
613 thaliana. Communications Biology. 2020;3(1):187.
614 31. Modliszewski JL, Wang H, Albright AR, Lewis SM, Bennett AR, Huang J, et al. Elevated temperature increases meiotic crossover
615 frequency via the interfering (Type I) pathway in Arabidopsis thaliana. Plos Genet. 2018;14(5):e1007384.
616 32. Lloyd A, Morgan C, H. Franklin FC, Bomblies K. Plasticity of meiotic recombination rates in response to temperature in
617 Arabidopsis. Genetics. 2018;208(4):1409-20.
618 33. Jin C, Sun L, Trinh HK, Danny G. Heat stress promotes haploid formation during CENH3-mediated genome elimination in
619 Arabidopsis. Plant Reproduction. 2023;36(2):147-55.
620 34. Ahmadli U, Kalidass M, Khaitova LC, Fuchs J, Cuacos M, Demidov D, et al. High temperature increases centromere-mediated
621 genome elimination frequency and enhances haploid induction in Arabidopsis. Plant Communications. 2023;4(3):100507.
622 35. Crhak Khaitova L, Mikulkova P, Pecinkova J, Kalidass M, Heckmann S, Lermontova I, et al. Heat stress impairs centromere
623 structure and segregation of meiotic chromosomes in Arabidopsis. eLife. 2024;12.
624 36. Ning Y, Liu Q, Wang C, Qin E, Wu Z, Wang M, et al. Heat stress interferes with formation of double-strand breaks and homolog
625 synapsis. Plant Physiology. 2021;185(4):1783-97.
626 37. Fu H, Zhao J, Ren Z, Yang K, Wang C, Zhang X, et al. Interfered chromosome pairing at high temperature promotes meiotic
627 instability in autotetraploid Arabidopsis. Plant Physiology. 2022;188(2):1210-28.

628 38. Lei X, Ning Y, Eid Elesawi I, Yang K, Chen C, Wang C, et al. Heat stress interferes with chromosome segregation and cytokinesis
629 during male meiosis in Arabidopsis thaliana. Plant Signaling & Behavior. 2020;15(5):1746985.
630 39. Chen Y, Dubois M, Vermeersch M, Inzé D, Vanhaeren H. Distinct cellular strategies determine sensitivity to mild drought of
631 Arabidopsis natural accessions. Plant Physiology. 2021;186(2):1171-85.
632 40. Lardon R, Wijnker E, Keurentjes J, Geelen D. The genetic framework of shoot regeneration in Arabidopsis comprises master
633 regulators and conditional fine-tuning factors. Communications Biology. 2020;3(1):549.
634 41. Taghavi Namin S, Esmaeilzadeh M, Najafi M, Brown TB, Borevitz JO. Deep phenotyping: deep learning for temporal
635 phenotype/genotype classification. Plant Methods. 2018;14(1):66.
636 42. Schulz E, Tohge T, Zuther E, Fernie AR, Hincha DK. Natural variation in flavonol and anthocyanin metabolism during cold
637 acclimation in Arabidopsis thaliana accessions. Plant, Cell and Environment. 2015;38(8):1658-72.
638 43. Zhu L, Fernández-Jiménez N, Szymanska-Lejman M, Pelé A, Underwood CJ, Serra H, et al. Natural variation identifies SNI1,
639 the SMC5/6 component, as a modifier of meiotic crossover in Arabidopsis. Proc Natl Acad Sci U S A. 2021;118(33).
640 44. Sidhu GK, Fang C, Olson MA, Falque M, Martin OC, Pawlowski WP. Recombination patterns in maize reveal limits to crossover
641 homeostasis. Proc Natl Acad Sci U S A. 2015;112(52):15982-7.
642 45. Ziolkowski PA, Underwood CJ, Lambing C, Martinez-Garcia M, Lawrence EJ, Ziolkowska L, et al. Natural variation and dosage
643 of the HEI10 meiotic E3 ligase control Arabidopsis crossover recombination. Genes & Development. 2017;31(3):306-17.
644 46. Lasky JR, Des Marais DL, Lowry DB, Povolotskaya I, McKay JK, Richards JH, et al. Natural variation in abiotic stress responsive
645 gene expression and local adaptation to climate in Arabidopsis thaliana. Molecular Biology and Evolution. 2014;31(9):2283-96.
646 47. Schiavon M, Zhang L, Abdel-Ghany SE, Pilon M, Malagoli M, Pilon-Smits EAH. Variation in copper tolerance in Arabidopsis
647 thaliana accessions Columbia, Landsberg erecta and Wassilewskija. Physiologia Plantarum. 2007;129(2):342-50.
648 48. Choi WG, Barker RJ, Kim SH, Swanson SJ, Gilroy S. Variation in the transcriptome of different ecotypes of Arabidopsis thaliana
649 reveals signatures of oxidative stress in plant responses to spaceflight. American Journal of Botany. 2019;106(1):123-36.
650 49. Liu B, De Storme N, Geelen D. Gibberellin induces diploid pollen formation by interfering with meiotic cytokinesis. Plant
651 Physiology. 2017;173(1):338-53.
652 50. Kurzbauer M-T, Janisiw MP, Paulin LF, Prusén Mota I, Tomanov K, Krsicka O, et al. ATM controls meiotic DNA double-strand
653 break formation and recombination and affects synaptonemal complex organization in plants. Plant Cell. 2021.
654 51. Zhao J, Gui X, Ren Z, Fu H, Yang C, Wang W, et al. ATM-mediated double-strand break repair is required for meiotic genome
655 stability at high temperature. Plant Journal. 2023;114(2):403-23.
656 52. Cai H, Zhao L, Wang L, Zhang M, Su Z, Cheng Y, et al. ERECTA signaling controls Arabidopsis inflorescence architecture through
657 chromatin-mediated activation of PRE1 expression. New Phytologist. 2017;214(4):1579-96.
658 53. Meng X, Wang H, He Y, Liu Y, Walker JC, Torii KU, et al. A MAPK cascade downstream of ERECTA receptor-like protein kinase
659 regulates Arabidopsis inflorescence architecture by promoting localized cell proliferation. Plant Cell. 2012;24(12):4948-60.
660 54. Lyu YS, Shao YJ, Yang ZT, Liu JX. Quantitative proteomic analysis of ER stress response reveals both common and specific
661 features in two contrasting ecotypes of Arabidopsis thaliana. International journal of molecular sciences. 2020;21(24).
662 55. Zhang SS, Yang H, Ding L, Song ZT, Ma H, Chang F, et al. Tissue-specific transcriptomics reveals an important role of the
663 unfolded protein response in maintaining fertility upon heat stress in Arabidopsis. Plant Cell. 2017;29(5):1007-23.
664 56. Xue M, Wang J, Jiang L, Wang M, Wolfe S, Pawlowski WP, et al. The number of meiotic double-strand breaks influences
665 crossover distribution in Arabidopsis. Plant Cell. 2018;30(10):2628-38.
666 57. Sanchez-Moran E, Santos JL, Jones GH, Franklin FC. ASY1 mediates AtDMC1-dependent interhomolog recombination during
667 meiosis in Arabidopsis. Genes & Development. 2007;21(17):2220-33.
668 58. France MG, Enderle J, Röhrig S, Puchta H, Franklin FCH, Higgins JD. ZYP1 is required for obligate cross-over formation and
669 cross-over interference in Arabidopsis. Proc Natl Acad Sci U S A. 2021;118(14).
670 59. Capilla-Pérez L, Durand S, Hurel A, Lian Q, Chambon A, Taochy C, et al. The synaptonemal complex imposes crossover
671 interference and heterochiasmy in Arabidopsis. Proc Natl Acad Sci U S A. 2021;118(12):e2023613118.

60. Higgins JD, Armstrong SJ, Franklin FCH, Jones GH. The Arabidopsis MutS homolog AtMSH4 functions at an early step in recombination: evidence for two classes of recombination in Arabidopsis. Genes & Development. 2004;18(20):2557-70.
61. Yao Y, Li X, Chen W, Liu H, Mi L, Ren D, et al. ATM promotes RAD51-mediated meiotic DSB repair by inter-sister-chromatid recombination in Arabidopsis. Front Plant Sci. 2020;11:839.
62. Draeger TN, Rey MD, Hayta S, Smedley M, Martin AC, Moore G. DMC1 stabilizes crossovers at high and low temperatures during wheat meiosis. Front Plant Sci. 2023;14:1208285.
63. Draeger T, A CM, Alabdullah AK, Pendle A, Rey MD, Shaw P, et al. Dmc1 is a candidate for temperature tolerance during wheat meiosis. Theoretical and Applied Genetics. 2019.
64. Grelon M, Vezon D, Gendrot G, Pelletier G. AtSPO11-1 is necessary for efficient meiotic recombination in plants. The EMBO journal. 2001;20(3):589-600.
65. Cromer L, Heyman J, Touati S, Harashima H, Araou E, Girard C, et al. OSD1 promotes meiotic progression via APC/C inhibition and forms a regulatory network with TDM and CYCA1;2/TAM. Plos Genet. 2012;8(7):e1002865.
66. Schindfessel C, Jin C, Geelen D. Heat induced male meiotic restitution and sexual polyploidisation through natural variation of the Arabidopsis cyclin TAM/CYCA1;2. bioRxiv. 2022:2022.08.11.503651.
67. Prusicki MA, Keizer EM, van Rosmalen RP, Komaki S, Seifert F, Müller K, et al. Live cell imaging of meiosis in Arabidopsis thaliana. eLife. 2019;8:e42834.
68. Cromer L, Jolivet S, Horlow C, Chelysheva L, Heyman J, De Jaeger G, et al. Centromeric cohesion is protected twice at meiosis, by SHUGOSHINs at anaphase I and by PATRONUS at interkinesis. Current Biology. 2013;23(21):2090-9.
69. Zamariola L, De Storme N, Vannerum K, Vandepoele K, Armstrong SJ, Franklin FC, et al. SHUGOSHINs and PATRONUS protect meiotic centromere cohesion in Arabidopsis thaliana. Plant Journal. 2014;77(5):782-94.
70. Yuan G, Ahootapeh BH, Komaki S, Schnittger A, Lillo C, De Storme N, et al. PROTEIN PHOSHATASE 2A B'α and β maintain centromeric sister chromatid cohesion during meiosis in Arabidopsis. Plant Physiology. 2018;178(1):317-28.
71. Cromer L, Jolivet S, Singh DK, Berthier F, De Winne N, De Jaeger G, et al. Patronus is the elusive plant securin, preventing chromosome separation by antagonizing separase. Proc Natl Acad Sci U S A. 2019;116(32):16018-27.
72. Khan ZH, Agarwal S, Rai A, Memaya MB, Mehrotra S, Mehrotra R. Co-expression network analysis of protein phosphatase 2A (PP2A) genes with stress-responsive genes in Arabidopsis thaliana reveals 13 key regulators. Sci Rep-Uk. 2020;10(1):21480.
73. Yamamoto A, Hiraoka Y. Monopolar spindle attachment of sister chromatids is ensured by two distinct mechanisms at the first meiotic division in fission yeast. The EMBO journal. 2003;22(9):2284-96.
74. Chan A, Cande WZ. Maize meiotic spindles assemble around chromatin and do not require paired chromosomes. Journal of Cell Science. 1998;111(23):3507-15.
75. Khodjakov A, Cole RW, McEwen BF, Buttle KF, Rieder CL. Chromosome fragments possessing only one kinetochore can congress to the spindle equator. Journal of Cell Biology. 1997;136(2):229-40.
76. Rebollo E, Arana P. A comparative study of orientation at behavior of univalent in living grasshopper spermatocytes. Chromosoma. 1995;104(1):56-67.
77. Hunt P, LeMaire R, Embury P, Sheean L, Mroz K. Analysis of chromosome behavior in intact mammalian oocytes: monitoring the segregation of a univalent chromosome during female meiosis. Human molecular genetics. 1995;4(11):2007-12.
78. Xue Z, Liu C, Shi W, Miao Y, Shen Y, Tang D, et al. OsMTOPVIB is required for meiotic bipolar spindle assembly. Proc Natl Acad Sci U S A. 2019;116(32):15967-72.
79. Couteau F, Belzile F, Horlow C, Grandjean O, Vezon D, Doutriaux MP. Random chromosome segregation without meiotic arrest in both male and female meiocytes of a dmc1 mutant of Arabidopsis. Plant Cell. 1999;11(9):1623-34.
80. Armstrong SJ, Jones GH. Meiotic cytology and chromosome behaviour in wild‐type Arabidopsis thaliana. Journal of Experimental Botany. 2003;54(380):1-10.
81. Chelysheva L, Grandont L, Vrielynck N, Guin Sl, Mercier R, Grelon M. An easy protocol for studying chromatin and recombination protein dynamics during Arabidopsis thaliana meiosis: immunodetection of cohesins, histones and MLH1.

716 Cytogenetic and Genome Research. 2010;129(1/3):143-53.
717 82. Wang Y, Cheng Z, Lu P, Timofejeva L, Ma H. Molecular cell biology of male meiotic chromosomes and isolation of male
718 meiocytes in Arabidopsis thaliana. Methods in molecular biology (Clifton, NJ). 2014;1110:217-30.
719

720 **Supporting Information**

721 Fig S1. Heat stress does not affect microtubule organization during prophase I in *Arabidopsis thaliana.*

722 Fig S2. Flower architectures in Col, L*er* and Col/L*er* hybrids.

723 Fig S3. Correlation analysis of synapsis, bivalent formation, and segregation of homologs at anaphase I in Col, L*er* and

724 Col/L*er* hybrids.

725 Fig S4. Representative images of meiotic chromosomes from anaphase I to metaphase II in wild-type Arabidopsis.

726 Table S1. Primers used in this study.

727